UNIVERSITÀ DEGLI STUDI DI MILANO
Dipartimento di Scienze Farmacologiche e Biomolecolari
Dottorato in Scienze Farmacologiche Sperimentali e Cliniche
XXXIII Ciclo – BIO/14

STUDY ON THE HDL::LCAT INTERACTION AND INSIGHTS INTO LCAT PHARMACOLOGICAL MODULATION

Tutor: Prof. Laura Calabresi
Co-Tutor: Prof. Ivano Eberini

Tommaso LAURENZI
Matr. N. 12039

A.A. 2019–2020

TABLE OF CONTENTS

ABSTRACT

English version

Lecithin:cholesterol-acyl-transferase (LCAT) plays a major role in cholesterol metabolism as it is the only extracellular enzyme able to esterify cholesterol. LCAT activity is required for lipoprotein remodeling and, most specifically, for the growth and maturation of HDLs. In fact, genetic alterations affecting LCAT functionality may cause a severe reduction in plasma levels of HDL-cholesterol with important clinical consequences, for which, at present, no optimal treatment is available.

Within this project, we ultimately aim at establishing landmarks for future structure-based drug-discovery of novel small-molecule activators able to rescue the defective enzyme in LCAT deficiency patients. To this end, we thoroughly studied the LCAT::HDL recognition and activation mechanism and investigated some aspects of LCAT pharmacological modulation.

Although several hypotheses were formulated, the exact molecular recognition mechanism between LCAT and HDLs is still unknown. We employed a combination of structural bioinformatics procedures to deepen the insights into the HDL-LCAT interplay that promotes LCAT activation and cholesterol esterification. We have generated a *data*-driven model of reconstituted HDL (rHDL) and studied the dynamics of an assembled rHDL::LCAT supramolecular complex, pinpointing the conformational changes originating from the interaction between LCAT and apolipoprotein A-I (apoA-I) that are necessary for LCAT activation. Specifically, we propose a mechanism in which the *anchoring* of LCAT *lid* to apoA-I helices allows the formation of a hydrophobic *hood* that expands LCAT active site and shields it from the solvent, allowing the enzyme to process large hydrophobic substrates.

Through the atomistic knowledge gained from our modeling work, we then studied the *mechanism-of-action* of some members of two known classes of small-molecule LCAT modulators and their interaction with a subset of LCAT mutants, rationalizing the bases for the future design of novel activators characterized by higher efficacy.

<ins>*Versione in Italiano*</ins>

La lecitina:colesterolo-acil-transferasi (LCAT) svolge un ruolo importante nel metabolismo del colesterolo, essendo l'unico enzima extracellulare in grado di esterificare il colesterolo. L'attività di LCAT è necessaria per il rimodellamento delle lipoproteine e, più specificamente, per la crescita e la maturazione delle lipoproteine ad alta densità (HDL). Infatti, alterazioni genetiche che interessano la funzionalità di LCAT possono causare una grave riduzione dei livelli plasmatici di colesterolo HDL con importanti conseguenze cliniche, per le quali, al momento, non sono disponibili trattamenti risolutivi.

Nell'ambito di questo progetto, miriamo a definire i punti di riferimento per la futura scoperta, con un approccio basato sulla struttura molecolare, di nuovi attivatori che possano essere utilizzate come farmaci in grado di ripristinare l'enzima difettivo nei pazienti con sindromi da deficienza di LCAT. A tal fine, abbiamo studiato a fondo il meccanismo di riconoscimento e di attivazione del complesso LCAT::HDL e studiato alcuni aspetti della modulazione farmacologica di LCAT.

Nonostante siano state formulate diverse ipotesi, l'esatto meccanismo di riconoscimento molecolare tra LCAT e le HDL è ancora sconosciuto. Abbiamo utilizzato una combinazione di procedure bioinformatiche strutturali per approfondire le conoscenze sull'interazione HDL-LCAT che promuove l'attivazione di LCAT e l'esterificazione del colesterolo. Abbiamo generato un modello, basato su dati sperimentali, di una lipoproteina HDL ricostituita (rHDL), assemblato e studiato la dinamica del complesso sovramolecolare rHDL::LCAT, individuando i cambiamenti conformazionali originati dall'interazione tra LCAT e apolipoproteina A-I (apoA-I) che sono necessari per l'attivazione di LCAT. In particolare, proponiamo un meccanismo in cui l'ancoraggio del *lid* di LCAT alle eliche centrali di apoA-I permette la formazione di un cappuccio idrofobico che espande il sito attivo di LCAT e lo protegge dal solvente, permettendo all'enzima di processare substrati idrofobici di grandi dimensioni.

Attraverso la conoscenza atomistica acquisita dal nostro lavoro di modellizzazione, abbiamo poi studiato il meccanismo d'azione di alcuni membri di due classi note di modulatori di LCAT e la loro interazione con un sottoinsieme di mutanti LCAT, ponendo le basi per la progettazione futura di nuovi attivatori caratterizzati da maggiore efficacia.

1 INTRODUCTION

1.1 LCAT

Lecithin:cholesterol-acyl-transferase (LCAT) is a 67 kDa plasmatic protein of the α/β-hydrolase family synthesized mainly in the liver and in lower amounts also in brain, testes and kidneys. It circulates in plasma reversibly bound to lipoproteins, where it catalyzes the esterification of free cholesterol (FC) through a two-step reaction mechanism that involves the hydrolysis of a phospholipid *sn*-1 or *sn*-2 alkyl chain and its transfer to FC. Cholesteryl esters (CEs) are then removed from the surface and accumulate within the lipoproteins core, allowing the particle to store larger amounts of cholesterol. Being the only extracellular enzyme able to catalyze cholesterol esterification, LCAT plays a crucial role in the maturation, remodeling and function of lipoproteins (1,2). Although LCAT is also active on apoB-containing lipoproteins, apoA-containing high-density lipoproteins (HDLs), the primary effectors of reverse cholesterol transport, are its preferential substrate and their principal protein constituent, apolipoprotein A-I (apoA-I), seems to be its strongest activator. Indeed, LCAT is required for the maturation and functionality of discoidal nascent pre-β-HDLs, that grow into spherical, mature, HDLs as they incorporate CEs produced by LCAT: while FC diffuses from the membranes of peripheral cells (including arterial walls macrophages) to nascent HDLs through the membrane ABCA1 transporter, LCAT preserves the concentration gradient by removing FC from the HDL surface (3).

Although the role of HDL in the prevention of coronary heart diseases is still debated, elucidating the role of LCAT in HDL-mediated reverse cholesterol transport remains a central issue that could aid in the treatment of cardiovascular diseases (3). Mutations in the LCAT gene lead to two rare recessive syndromes, fish-eye disease (FED) and familial LCAT deficiency (FLD), characterized by decreasing levels in LCAT residual activity. Clinical manifestations of the disease include, corneal opacity, anemia, hypoalphalipoproteinemia and alterations in blood lipids and CEs levels

(4,5). In the case of FLD, alterations in HDLs maturation may result in the formation of abnormal multilamellar lipoproteins, LpX, which can cause nephropathy leading to life-threatening renal failure (6).

1.1.1 LCAT structure

Human LCAT gene (~ 4.4 kB on 16q22) encodes for a 416-amino acid glycoprotein preceded by a 24-amino acid long signal peptide (MW 4.9 kDa) (7). The gene is expressed mainly in the liver and to a lesser extent in brain, testis and kidneys (8). The synthetized protein is secreted in the plasma and circulates in a glycosylated form (N-linked and O-linked) for a total molecular mass of approximately 67kDa (1).

The high-resolution LCAT protein structure was experimentally determined in 2015 by Piper et al. (9), after the publication of remarkably accurate distant homology models (10,11), based on LCAT homology with other lipases, especially LPLA2. Indeed, LCAT is a member of the α/β hydrolase fold family, with a central domain consisting of six parallel β-strands surrounded by 5 α-helices and separated by loops (Figure 1). The active site containing the characteristic and conserved catalytic triad is found within this core region of the protein. The catalytic triad includes Ser181, Asp345 and His377, together with the oxyanion hole formed by backbone amide nitrogen atoms from Cys31 and Leu182 (9). The subdomain between residues 32–119 contains the disulfide bridge Cys50–Cys74 and was proposed as "lid" domain, typical of lipases. The lid frequently plays dual roles, blocking/allowing access to the active site through conformational changes and being involved in interfacial activation in the presence of a lipid-water interface. However, in LCAT, this subdomain does not cover the active site, although it has been shown that this region is required for interfacial activation and it is essential for the binding to lipoprotein surface (1,12); it is therefore referred to as the *membrane-binding domain* (MBD) of LCAT. The *actual* lid of LCAT is formed by a flexible loop between residues 225–250 (13) and it is part of the *cap* subdomain, formed by residues 214–303 and residues 319–344.

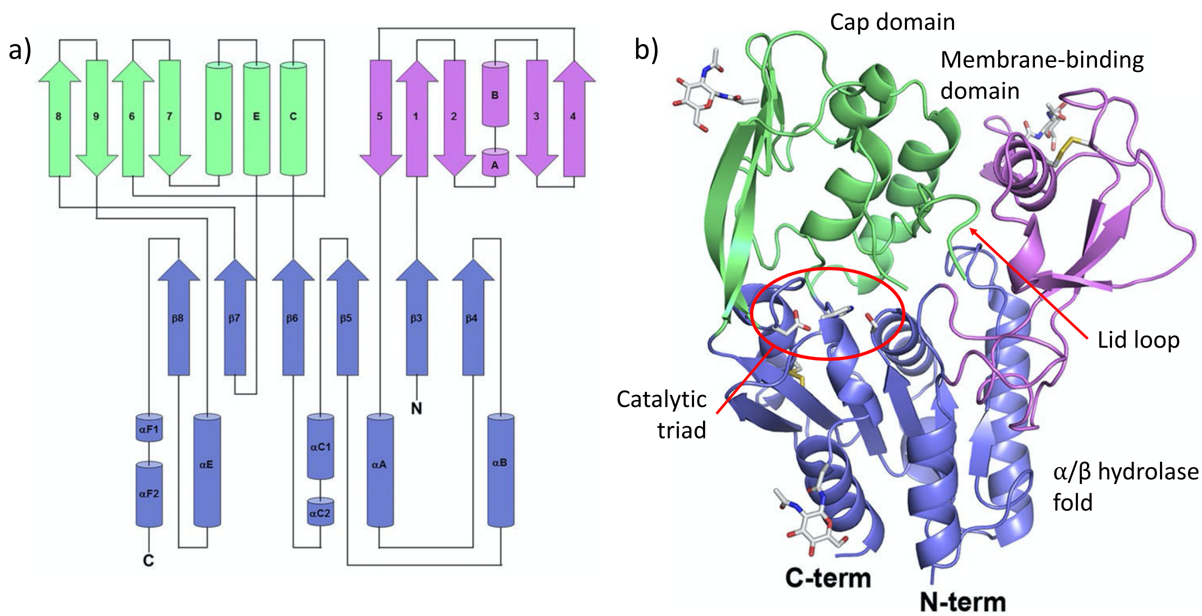

Figure 1 – LCAT structure. a) Topology and b) structure of lecithin:cholesterol-acyl-transferase; α/β-hydrolase core (blue), cap domain (green), membrane-binding domain (purple).

1.1.2 LCAT reaction and substrates

LCAT reaction cycle comprises two different catalytic reactions: phospholipase and acyltransferase activity. Its most important physiologic reaction is to produce cholesteryl esters by converting cholesterol and phosphatidylcholine (PC) (lecithin) into cholesteryl ester and lysophosphatidylcholine (lysoPC). As depicted in Figure 2, LCAT performs a multistep reaction starting with the cleavage of the fatty acid in *sn*-2 position of lecithin resulting in the acylation of Ser181, then the fatty acid is transferred to the free 3-β hydroxyl group of cholesterol (transesterification), generating cholesteryl ester (CE) (1). Although human LCAT preferentially transfers *sn*-2 acyl chains of PC to cholesterol, *sn*-1 acyl chains may also be utilized (14).

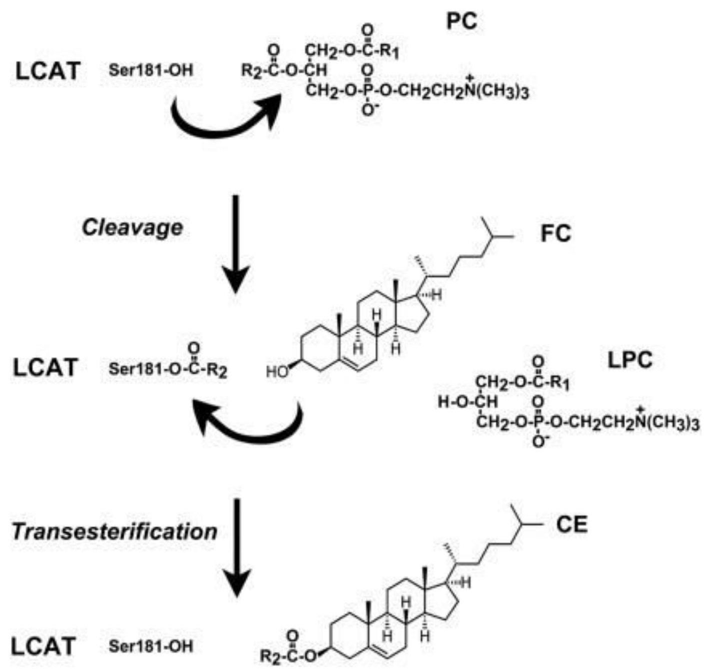

Figure 2 – LCAT reaction. First, LCAT cleaves the sn-2 fatty acid of phoshatidylcholine (PC) with formation of lysophosphatidilcholine (LPC). Then, the fatty acid, bound to Ser181 of LCAT is transferred to the hydroxyl group of free cholesterol (FC) to give a cholesteryl ester (CE).

Besides PC, LCAT can use other phospholipids containing 18:1 or 18:2 fatty acids (15), such as phosphatidylethanolamine (PE), but it has no activity on other phospholipids or acyl donors, such as phosphatidylserine or diacylglycerol (16).

Small, discoidal apoA-I-containing pre-β-HDLs (described in *HDL function and metabolism*) are the preferential substrate of LCAT (17), however, although with lesser affinity, LCAT is able to trans-esterify cholesterol also on apoB-containing lipoproteins (18). The activity of LCAT on these two different substrates is usually referred to as α- and β-LCAT activity. Measurement of affinity of human LCAT for different substrate showed that it was 2.3 to 4-fold higher for HDLs compared to low-density lipoproteins (LDLs), with relative reactivity (appVmax/app Km) of 6.5%, 1.3% and 16% for LDL, HDL2 and HDL3 compared to rHDL (19). Despite β-LCAT activity, apoB-containing lipoproteins mainly acquire CE by Cholesteryl Ester Transfer Protein (CETP), which exchanges CE (made by LCAT) for triglycerides between HDL and LDL. Either way, LCAT is the main source of CE on apoB-containing lipoproteins. Other CE are produced by one intracellular enzyme Acyl-CoA:Cholesterol Acyltransferase (ACAT) in the liver and intestine when chylomicrons and VLDL are secreted (20).

1.1.3 Genetic LCAT deficiency

The effects of genetic impairment of LCAT activity were first described in 1967 by Norum and Gjone (21). Carriers of LCAT gene mutations showed a wide variety of phenotypic presentation. Most homozygous carriers develop corneal opacities, hemolytic anemia and a chronic and progressing renal insufficiency, often resulting in end-stage renal disease. Heterozygous subjects show a mild phenotype, supporting the evidence that LCAT deficiency is an autosomal recessive disorder. Loss-of-function mutations in both alleles, depending on the type, can lead to two distinct syndromes: familial LCAT deficiency (FLD) and fish-eye disease (FED). Both are characterized by low HDL-cholesterol (HDL-c) in plasma, but other clinical and biochemical features can be widely different (5). While in FLD the lack of LCAT impair the ability of the enzyme to esterify cholesterol on both HDL and LDL, in FED the enzymatic activity on LDL and VLDL is preserved. The direct consequence is that FLD have a very little amount of CE with high FC in all lipoproteins fractions, while FED have a subnormal CE/FC ratio with concentration of CE in apoB-containing lipoproteins, that are present in normal plasmatic levels. Among other characteristics, corneal opacity is common in both FLD and FED, whereas anaemia, proteinuria and renal disease are clinical features of FLD (22).

The impairment of HDL-c metabolism leads to formation of abnormal multilamellar particles called lipoprotein-X (LpX): vesicles comprised of phospholipid and free-cholesterol bilayers surrounding an aqueous core. These particles can accumulate in the kidneys causing glomerular sclerosis and a progressive renal insufficiency which ultimately leads to renal failure, which represents the first cause of morbidity and mortality in FLD-affected patients (6).

The differential diagnosis of FLD and FED in homozygous or compound heterozygous can only be made by the measurement of the ability of LCAT to esterify the FC on endogenous lipoproteins (α-LCAT plus β-LCAT activity) and on synthetic HDL (α-LCAT activity) (23). The classification of heterozygous subjects can be made by transient expression of LCAT mutants in cultured cells and measurement of LCAT concentration and activities in cell media (24). The prevalence of the disease is below 1:1,000,000 and more than 80 mutations in LCAT gene have been identified (5).

Specific treatment for genetic LCAT deficiency is not currently available. Therapy is mainly aimed at correcting the dyslipidemia and at delaying the evolution of chronic nephropathy, with changes in lifestyle and diet and anti-hypertensive treatment to avoid proteinuria (25). Moreover, despite kidney transplantation, the disease can reoccur in transplanted tissue (26).

Since LCAT has a relatively long half-life and does not require any specific tissue delivery, LCAT deficiencies are good candidates for enzyme replacement therapy (ERT). Treatment with recombinant human LCAT (rhLCAT) in mouse model of LCAT deficiency and the first-in-human treatment provided encouraging results (27–29). Although effective, being a biological product, rhLCAT is expensive, requires infusion, and can cause immunogenicity in treated patients, which is a relevant issue in chronic treatments. Development of a *small-molecule*-based therapy could have major advantages to patients compared to ERT, including an oral administration route and no need for inpatient treatment, leading to an improved quality of life and lower social costs.

1.1 High-density lipoproteins

1.1.1 HDL function and metabolism

HDLs are a highly heterogeneous lipoprotein family whose most important function is to promote the removal of cholesterol from peripheral cells and allow its redistribution or excretion through bile acids in a process called reverse cholesterol transport (RCT).

HDLs prevalently form peripherally starting from circulating lipid-free apoA-I, which is synthesized mainly by the liver (30) and, to a lesser extent, by the small intestine (31), from which it is secreted as components of triglyceride-rich lipoproteins. After conversion of pro-apoA-I by plasma metalloprotease (32), the mature lipid free-apoA-I acquires phospholipids and cholesterol through the interaction with the ATP binding cassette transporter A1 (ABCA1), to form pre-β-HDL (33). These particles are classified according to charge measurements on agarose gel and represent the initial or *nascent* stage of the HDLs. Pre-β-HDLs have a discoidal shape consisting of a bilayer of phospholipids lacking the non-polar core; two antiparallel amphipathic helices of apoA-I surround the disk, with polar residues facing the aqueous phase and non-polar residues facing the acyl chains of the lipid bilayer (34). Once in the circulation, pre-β-HDL are the preferential substrate of LCAT (Figure 3), that converts lecithin and cholesterol into lysolecithin and cholesteryl esters, using apoA-I as cofactor (1). The cholesterol esters generated by LCAT are more hydrophobic than free cholesterol and thus migrate into the hydrophobic core of the lipoprotein, with the resulting conversion of small, discoidal pre-β-HDL into larger, spherical, α-migrating HDL (α-HDL) (1). Mature HDLs have a globular shape, where the central core is composed by low-density non-polar lipids (triglycerides and cholesteryl esters) surrounded by a monolayer of polar lipids (phospholipids and unesterified cholesterol) and high-density apolipoproteins (35). LCAT thus plays a central role in intravascular HDL metabolism and in the determination of plasma HDL level. The α-HDL produced by LCAT (HDL_3) interact in the plasma with CETP, that exchanges cholesteryl esters for triglycerides between HDL and triglyceride-rich lipoproteins, generating large cholesteryl ester-poor and triglyceride-rich HDL particles (HDL_2) (36). The CETP-mediated exchange of cholesteryl esters with apoB-containing triglyceride-rich lipoproteins ultimately contributes to the formation of lipid-poor/cholesterol-rich LDLs, that shuttle esterified cholesterol to the liver, where it can be converted and excreted in the form of bile acids (37), concluding the RCT cycle. Mature, large α-HDL particles can be converted back to pre-β-HDL through the action of PLTP and the endothelial and hepatic lipases, that hydrolyze triglycerides and phospholipids on HDL (Figure 3) (38). HDL particles may be then catabolized in liver and kidney, with the recycling of the protein component (39–41).

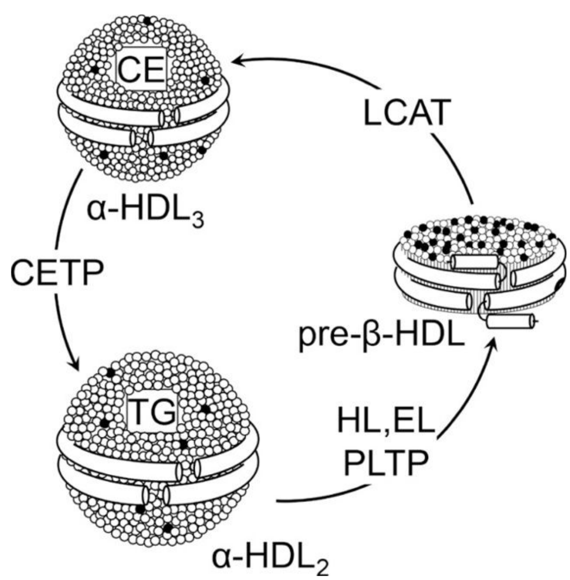

Figure 3 – HDL metabolism. LCAT esterifies free cholesterol located on the surface of pre-β-HDL. The cholesterol esters generated by LCAT migrate into the hydrophobic core of the lipoprotein due to their hydrophobicity, with the resulting conversion of pre-β-HDL into α-HDL3. The α-HDL3 produced by LCAT interact with cholesteryl ester transfer protein (CETP), that exchanges cholesteryl esters for triglycerides generating large cholesteryl ester-poor and triglyceride-rich HDL particles (α-HDL2). α-HDL2 can be

converted back to pre-β-HDL through a variety of lipases activities that hydrolyze triglycerides and phospholipids on HDL. CE, cholesteryl esters; TG, triglyceride; HL, hepatic lipase; EL, endothelial lipase; PLTP, phospholipid transfer protein.

1.1.2 Structure of apoA-I

Apolipoprotein A-I (apoA-I) accounts for 70% of HDL protein content, followed by apolipoprotein A-II (apoA-II) (20%). However, mature HDLs contain up to 48 or more proteins, including apoA-IV, apoCs, apoE, lecithin:cholesterol acyltransferase (LCAT), CETP, phospholipid transfer protein (PLTP), paraoxonase (PON), and platelet-activating factor acetylhydrolase (PAF-AH) (35,42,43). ApoA-I is required to stabilize the HDL particle structure, interact with the ABCA-I transporter (44), activate LCAT (45) and represents the ligand for the hepatic scavenger receptor B1 (46).

ApoA-I is a 28 kDa 243-residue protein encoded by two exons in the APOA1 gene. Residues 1–43, encoded by exon-3, contain a globular amino-terminal domain, while residues 44–243, encoded by exon-4 (47), contain 10 tandem 11/22-residue repeats, punctuated by prolines, thought to form lipid-binding class A amphipathic helices that represent the fundamental lipid-binding motif (48–50) (Figure 4a). All 10 repeats in this domain are associated with lipid in the HDL particle (51).

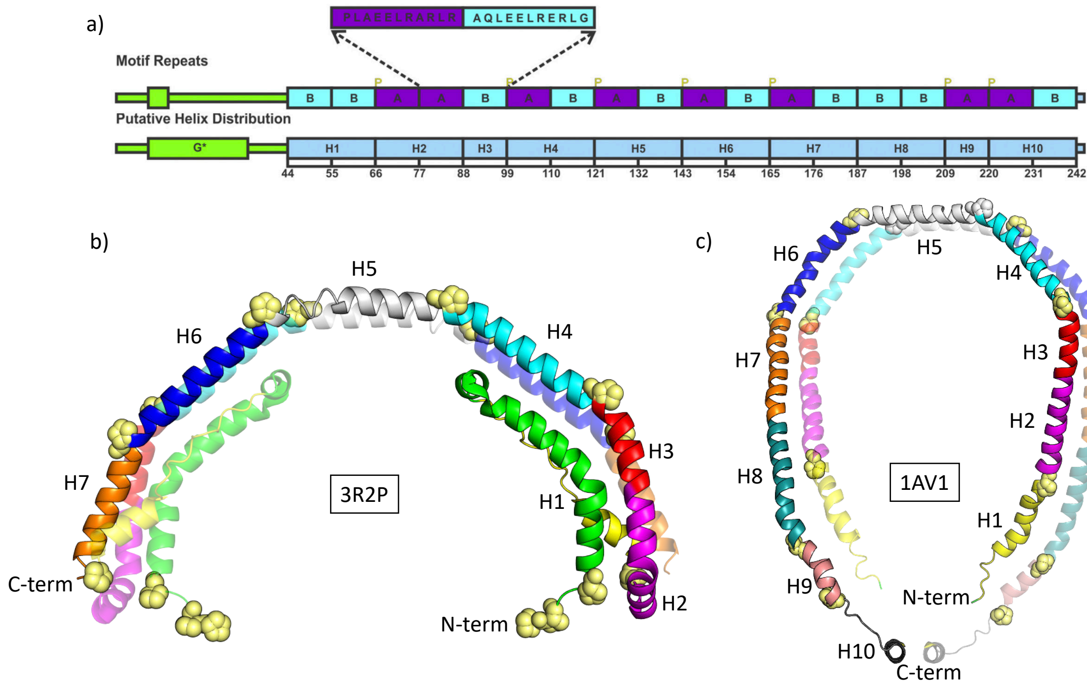

Figure 4 – apoA-1 structure. a) illustrations of the helix distribution and motif repeats from sequence analysis (52); b) 2.2-Å resolution *3R2P* crystal structure of Δ(185–243)apoA-I forming a half-circle antiparallel dimer centered on helix 5 (H5); c) 4-Å resolution *1AV1* crystal structure of Δ (1–43)apo A-I containing residues 44–243 (exon 4) forming a 2-helix bundle with an elliptical ring shape.

ApoA-I exists in lipid-free, lipid-poor, and lipid-bound states and possess a flexible and adaptable structure that challenges high resolution structural studies. Two major landmarks in the determination of the structure of apoA-I in HDLs were reached after the publication of N- and C-terminally truncated structure of delipidated apoA-I by Borhani et al. (1997)(53) (Figure 4c) and Mei and Atkinson (2011) (54) (Figure 4b); however, apoA-I crystallographic structures depict the protein likely far from its physiological folding and the resolution of the complete lipid-bound structure of apoA-I is still a major challenge of structural biochemistry. In the history of apoA-I structural studies, several computer models backed up by experimental data were proposed. Since the work of Koppaka et al. (1999) (55), the so-called *double belt* arrangement (opposed to the *picket-fence* model) has been established almost unambiguously. Further work by Segrest et al. (1999) (56) has then proposed the antiparallel LL (left-to-left) orientation of apoA-I chains with a 5/5 registry, based on computational calculations; their findings were then supported by the cross-linking/MS experiments of Silva et al. (2005) (57). Since then, other computational models have been proposed, showing significant differences albeit sharing the common configuration of double belt in LL/5 registry. Notably, the *solar flare* model proposed by Wu et al. (2007) (58), which identified, via hydrogen-deuterium exchange experiments, solvent-exposed protruding bulges in apoA-I chains (corresponding to residues 159–180) that were proposed to activate LCAT; the *belt buckle* model, from Bhat et al. (2008) (59), where cross-linking/MS data were collected on 145 POPC rHDL particles, showing that N- and C-termini folded back onto apoA-I helices; the *looped belt* model, by Martin et al. (2006) (60), generated by performing EPR and FRET experiments on 100 POPC rHDLs, suggesting the presence of a central loop region comprised by residues 133–146. Another model was proposed by Wu et al. (2009) (61) in accordance with FRET, ESR and cross-linking/MS data obtained by others; this model displayed apoA-I helices spiraling around a 100 POPC cylindrical core as a *double superhelix*; however, the reliability of this model was challenged by Jones et al. (2010) (62) who tested the thermodynamic and kinetic stability of the double superhelix via extensive coarse-grained and simulated-annealing molecular dynamics (MD) simulations.

2 AIMS

LCAT is a liver-secreted protein that circulates in plasma reversibly bound to lipoproteins, where its main function is to catalyze cholesterol esterification, transferring an acyl chain from phosphatidylcholine to free-cholesterol. Thus, LCAT is a fundamental protein in cholesterol metabolism and lipoprotein remodeling as it is required for the growth and maturation of HDLs, pivotal actors in the reverse cholesterol transport cycle, that allows the redistribution and excretion of excess cholesterol.

Loss-of-function mutations affecting the LCAT gene may therefore cause severe clinical consequences and lead to two distinct syndromes that differ by LCAT residual activity: familial LCAT deficiency (FLD) and fish-eye disease (FED). The impairment of HDL-cholesterol metabolism leads to formation of abnormal multilamellar particles (LpX) that can accumulate in the kidneys causing glomerular sclerosis. The first cause of morbidity and mortality in the LCAT deficiency syndrome is indeed a chronic and progressing renal insufficiency, often resulting in end-stage renal disease for which, at present, no optimal treatment is available. The viability of a small molecule-based approach to treat LCAT deficiencies would provide several advantages to patients in terms of an improved quality of life and lower social costs.

Since LCAT is active prevalently on the surface of HDLs, we need to consider the nature of HDL::LCAT interactions to gain an in-depth knowledge of LCAT activation and reaction mechanisms that will provide the bases for the study of pharmacological LCAT modulators.

The aim of this project is to provide an (r)HDL::LCAT *interaction model that would establish landmarks for structure-based drug-discovery of novel small-molecule* LCAT *activators to be used in the treatment of* LCAT *deficiency syndromes and cardiovascular diseases.*

To achieve our goal, this project was carried out according to the following outline:

Study of LCAT activation and reaction mechanism.

We utilized several computational techniques to investigate the HDL::LCAT interactions responsible for LCAT activation.

- First, we wanted to cross-validate an all-atom model of a reconstituted HDL (rHDL) with a 5/5 LL apoA-I orientation. The rHDL model was generated making use of available crystallographic structures and apoA-I::apoA-I cross-linking information. The model stability was assessed via molecular dynamics (MD) simulations and several structural information were used to validate our results.
- Then, we refined the available experimentally determined structures of LCAT to obtain a model that best resembles the structure of the physiologically active state of the protein.
- Finally, we assembled, tested and analyzed multiple rHDL::LCAT supramolecular complexes, fitting data originating from experimental cross-linking and mutagenesis studies. Here, we aim at elucidating the structural events occurring in the LCAT activation, substrate recognition and reaction cycle, with emphasis on the rHDL::LCAT interactions at play. Cooke et al (2018) (63) surveyed the literature for instances of apoA-I mutations that impact LCAT activation without affecting cholesterol efflux, thereby preserving the global lipoprotein structure; the authors found that natural and engineered point mutations in apoA-I that fit these criteria were concentrated in helices 4, 6, and 7. Since HDLs are composed of two antiparallel apoA-I chains centered on helix 5, helices 4/6 and 7/3 are paired. Starting from this information, and integrating with cross-linking experiments that

investigated proximal residues in apoA-I::LCAT, we wanted to pinpoint the residues responsible for the rHDL::LCAT interfacial recognition on both partners.

Study of LCAT pharmacological modulation.

- We investigated the mechanism-of-action of some members of two known classes of small-molecule LCAT modulators, including the analysis of their interaction with a subset of naturally occurring FLD LCAT mutants.
- Then, we integrated these results with the atomistic knowledge gained from our modeling work and individuated a set of potential novel LCAT modulators amenable to be further optimized and tested in vitro/in vivo.

3 MATERIALS AND METHODS

3.1 Structure preparation.

LCAT structures 5BV7, 5TXF and 6MVD were prepared using the “Structure preparation and refinement” panel of the Maestro program (Maestro, Schrödinger, LLC, New York, NY, 2018). This step consists in the protonation (pH 7), filling of missing side-chains/residues and hydrogen-bond optimization. Missing residues 236–242 of 5BV7, 240–141 of 5TXF and 235–243 of 6MVD, all within the lid-loop, were modelled using an *ab initio* method available in the module Prime of the same suite; since LCAT N- and C-termini were proven to be necessary for LCAT activity (64–66), residues 1–20 and 399–416 of 5BV7 and 5TXF structures were also modelled. Despite the high number of residues to be modeled *ab initio*, we do not expect that inaccuracies in the predicted structure of these residues could affect our MD simulations.

5BV7 and 5TXF structures were used to study LCAT lid-loop dynamics and LCAT::rHDL interactions, while the 6MVD structure was used to study LCAT::ligand interactions.

The PDB codes of utilized apoA-I structures are 3R2P (54), 1AV1 (53) and CNS (67). The latter is a *consensus* model of circulating delipidated apoA-I.

3.2 rHDL modelling.

To generate the apoA-I all-atom model we merged structural fragments of existing templates into a *chimeric* structure. Template patches were selected considering the following properties: i) residues are in alpha-helix secondary structure, ii) suitable orientation of amphipathic helices, iii) ability to confer a circular shape to the model. We used 3R2P as the main template; the first 36 residues of the missing C-terminus helices (residues 183–218) were reconstructed from the corresponding residues of 1AV1 structure, while residues 219–243 were shaped on 3R2P central helices (residues 156–182). Residues 1–37 of 3R2P folded N-terminus (residues 1–79) were remodeled using residues from: 3R2P central helices (residues 156–182), a small fragment of the *consensus* model (CNS) and residues 44–79 of 1AV1. Structure alignment algorithms were used to correctly position residue patches using 2 to 5 overlapping residues as a guide. Energy-based homology modelling (Prime, Schrödinger, LLC, New York, NY, 2018) was used as a tool to model N- and C-termini last residues onto 3R2P residues 156–182 and to *seal* the final patched model into a continuous chain. A single apoA-I chain was modelled in this way; to model the homodimeric supramolecular assembly, a duplicated image of the generated chain was aligned to residues 80–182 of the antiparallel chain of 3R2P. The lipid core of the rHDL was built from an equilibrated POPC bilayer extracted from a validated MD simulation. The lipids bilayer was trimmed to a circular disk of 164 POPC molecules with a diameter of 9.2 nm and symmetrically positioned at the center of the chimeric model by aligning the coordinates of reference centers of mass. Residues within 3 Å from the phospholipidic core were minimized to avoid steric clashes (Polak-Ribiere Conjugate Gradient with convergence on RMS gradient with a threshold of 0.5).

3.3 Molecular Dynamics simulations.

All MD simulations were performed with the Desmond Molecular Dynamics System (D. E. Shaw Research, New York, NY, 2018. Maestro-Desmond Interoperability Tools, Schrödinger, New York, NY, 2018) with the following base setting: timestep for close and far interactions, 300 K Nose-Hoover thermostat, Martina-Tobias-Klein barostat with isotropic coupling and a 9.0 Å cut-off for Coulombic interactions.

Folding of the apoA-I chains around the lipid core was achieved with a 100 ns restrained MD simulation to ensure the reproducibility of the simulation and consistency towards experimental structural data. Selected atom pairs were pulled together by a flat-bottomed distance restraints with a force constant of 0.15 kcal mol^{-1} $Å^{-1}$ and a distance threshold of 7.5 ± 7.5 Å. Atom pairs sets were chosen considering data from cross-linking experiments (57,61,68,69) (Figure 5 and Figure 7a).

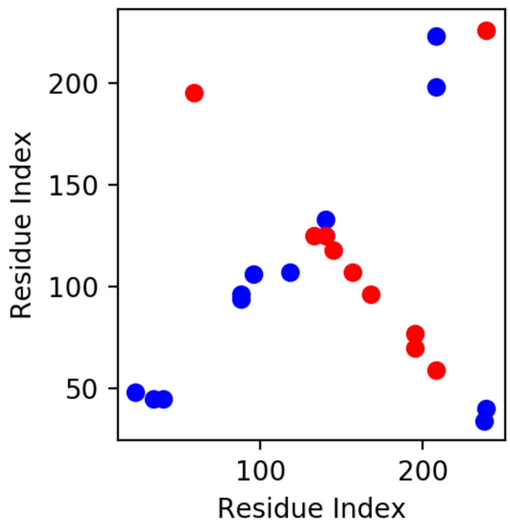

Figure 5 – apoA-I cross-link map. Inter-chain cross-links (red), intra-chain cross-links (blue).

POPC residues were restrained on Z axis with a force constant of 5 kcal mol^{-1} $Å^{-1}$ to prevent the formation of a lipid drop that would have hindered hydrophobic interactions with apoA-I amphipathic helices. All restraints were removed after 100 ns and the MD was extended up to 300 ns.

Simulations of LCAT, LCAT::Fab, rHDL::LCAT complexes and LCAT::DS-compound were all carried out with default settings.

3.4 Metadynamics.

A well-tempered metadynamics (wtMTD) simulation was set up to explore the energy landscape of the LCAT structure as a function of lid positioning. Two collective variables (CVs) were chosen to track the lid loop movements: 1) the dihedral angle formed by the centers of mass of the following groups: β6/β7 (214–303) and β7/αE (319–344) subdomains (the *cap* subdomain); the catalytic triad (181, 345, 377); the whole structure except the lid; the *tip* of the lid loop (232–238); 2) the distance between Cα of residues Met234 and Gly119. The height of the gaussian potential was set to 0.04 kcal mol^{-1}, with a *k*T of 5 kcal mol^{-1} and a deposition rate of 0.2 ps; a σ of 2.5° and 0.25 Å was set for the two CVs respectively. A 100.0 kcal mol^{-1} positional constraint was also applied to all Cα atoms, except for the lid loop (225–250) and the β3/αA (MBD) subdomain (32–119), to prevent the biasing potential to affect every atom included in the CVs definition, thus ensuring values of the CVs to depend on lid positioning only. The system was prepared using the LCAT open 5TXF structure.

Abduction of a phospholipid from the surface of the rHDL towards LCAT active site was carried out using standard MTD; settings: wall 20 Å, deposition rate 1 ps, σ of 0.1 Å, height of the gaussian potential 0.3 kcal mol^{-1}. Other default MD settings were kept as reported in the Molecular Dynamics paragraph.

3.5 Protein::protein docking.

The PIPER FFT-based protein::protein docking program (licensed by Schrödinger, New York, NY, 2018) was used to dock LCAT on the final rHDL model. The last frame (300 ns) of the rHDL model from the MD simulation was minimized and set as the *receptor*, while the open- and closed-lid conformations of LCAT, obtained from the largest wtMTD minima, were set as *ligands*.

Constraints were added to the docking protocol on the basis of experimental cross-linking and mutagenesis data: interactions with apoA-I residues 143–187 were favored by weighting the internal scoring function; at least one pair of residues observed in experimental cross-linking (70) were forced to stay within 12 Å. Poses were then analyzed and accepted or rejected on the basis of geometric considerations: i) proximity and orientation of LCAT active site towards phospholipid head groups, ii) contacts between LCAT β3/αA domain and lipids.

3.6 LCAT membrane-binding

To measure the strength of LCAT::membrane interaction the following MD protocol was employed:

1) First, the system was built using LCAT 6MVD structure, and a membrane containing POPC and CHOL in a 20:1 ratio. Two systems, with and without the co-crystalized ligand, were generated from the 6MVD structure; both systems were subject to the following steps.
2) A biased MD was used to *push* LCAT onto the membrane. A harmonic biasing potential, with a force constant of k = 0.3 kcal mol^{-1} Å^{-2}, was applied to LCAT MBD as a function of its distance from the center-of-mass of the membrane *upper* layer. The biasing potential was removed after 20 ns and the system was then equilibrated for 10 *ns*.
3) Steered MD was used to *pull* LCAT away from the membrane; the harmonic potential, with a force constant of k = 0.25 kcal mol^{-1} Å^{-2} was applied to LCAT center-of-mass as a function of its distance (projected on the Z axis) from a *virtual* reference moving away from the membrane perpendicularly (along the Z axis) with a constant speed v = 1 Å ns^{-1}. The force profile of LCAT detachment was then calculated as a function of LCAT Z-projected distance from its starting configuration according to Hooke's law.

3.7 LCAT ligand preparation and docking

Molecular docking was performed using Glide (Schrödinger Release 2018-4: Glide, Schrödinger, LLC, New York, NY, 2020). To discover novel allosteric activators able to bind within LCAT MBD, we screened a library of 91,001 "lead-like" compounds screened against a panel of early ADMET tests (including DMSO and water solubility, PAMPA, PGP and CYP inhibition) amenable for rapid hit-to-lead optimization. The "Elite-Synergy" library, provided by Asinex, is available at *http://www.asinex.com/wp-content/uploads/2021/02/2021-02-AsinexEliteSynergy-91001.zip*.

Ligands were prepared with the Schrödinger LigPrep utility. This step allows the generation of tautomers, stereoisomers and protonation state variants at pH 7±2 for each molecule.

DS-compound and LCAT 6MVD co-crystalized ligand were docked using the extra-precision XP algorithm. Asinex library compounds were docked using the virtual-screening-workflow procedure. This procedure docks ligands with algorithms of increasing accuracy (and computational cost); at each stage, the 10% of the top-scoring poses is passed to the following step, terminating with the XP algorithm.

4 RESULTS AND DISCUSSION

4.1 rHDL model

Since LCAT is active mainly on the surface of HDLs, where apoA-I is the main activator, understanding the interactions between LCAT, apoA-I and a lipid interface is crucial to picture LCAT activation and reaction mechanism. We chose to model a rHDL as this type of lipoprotein is the best simplified system to maintain general HDL properties, allowing the cross-validation between our models and experimental results.

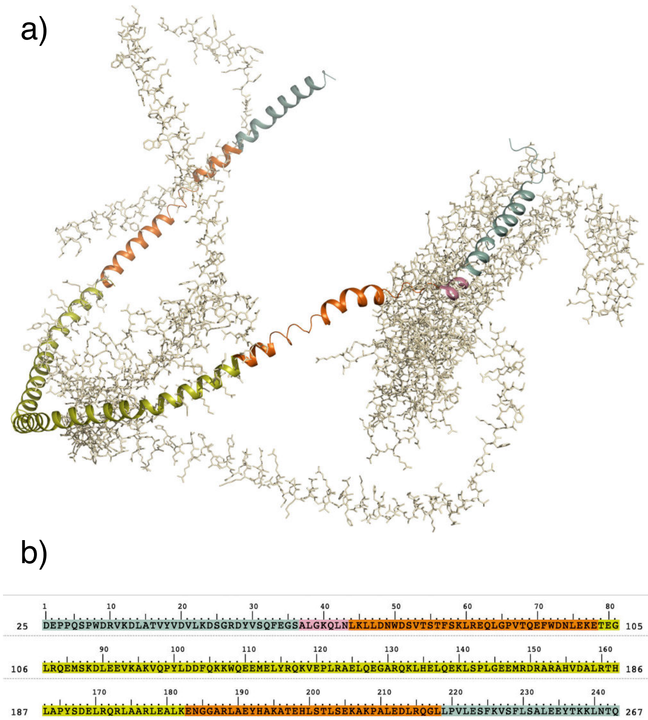

Figure 6 – ApoA-I chimeric model. a) Ribbon representation of the patched apoA-I chimeric model; residues not used in the model generation are shown in light gray; b) color coded apoA-I primary structure. Color code: 3R2P green, homology model blue, 1AV1 orange, CNS pink.

As experimentally resolved lipid-bound apoA-I structures are currently unavailable, we relied on lipid-free apoA-I crystallographic data (53,54). We aligned residue patches of three structures, 1AV1, 3R2P and CNS to reconstruct a full-atom model of a lipid-free apoA-I poised to wrap around a lipidic core (

Figure 6). A mixed protocol of *restrained* and *free* MD was then used to drive the folding of the modelled apoA-I chains around the lipid core (see Materials and Methods section).

During the course of the simulation, apoA-I chains rearranged to better adapt to the size of the lipid core by assuming a hybrid *zig-zag* conformation and exposing hydrophobic residues towards the lipid core (Figure 8a) while maintaining an 80 % α-helicity content. Computed tryptophan solvent accessible surface hindrance ($f_a = 80\%$) is also consistent with results by Guerini Rocco et al. (2009) (71). This measure is readily comparable with experimental data that measure, via fluorescent quenching methods, the amount of tryptophan surface area that is not exposed to the solvent. Indeed, this *accordion*-like conformation would allow apoA-I helices to stretch in order to accommodate larger amounts of lipids during HDLs maturation and growth.

ApoA-I N- and C-termini wrapped around the POPC bilayer within the first 20 ns of the simulation, as shown by the initial drop in the radius of gyration, which eventually stabilizes at 4.5 nm, consistently with literature data (71,72) (Figure 7b). The root-mean-square deviation (RMSD) profile of apoA-I residues indicates that the rHDL model reached a stable conformation within the first 100 ns (Figure 7); after the removal of distance restraints at 100 ns, more conformations become available for the system, which converges towards a new stable conformation between 200 ns and up to the end of the simulation (Figure 7); nonetheless, distances between restrained atoms are preserved ($\langle distance \rangle$ = 14.4 Å, SD = 3.2 Å) (Figure 7f).

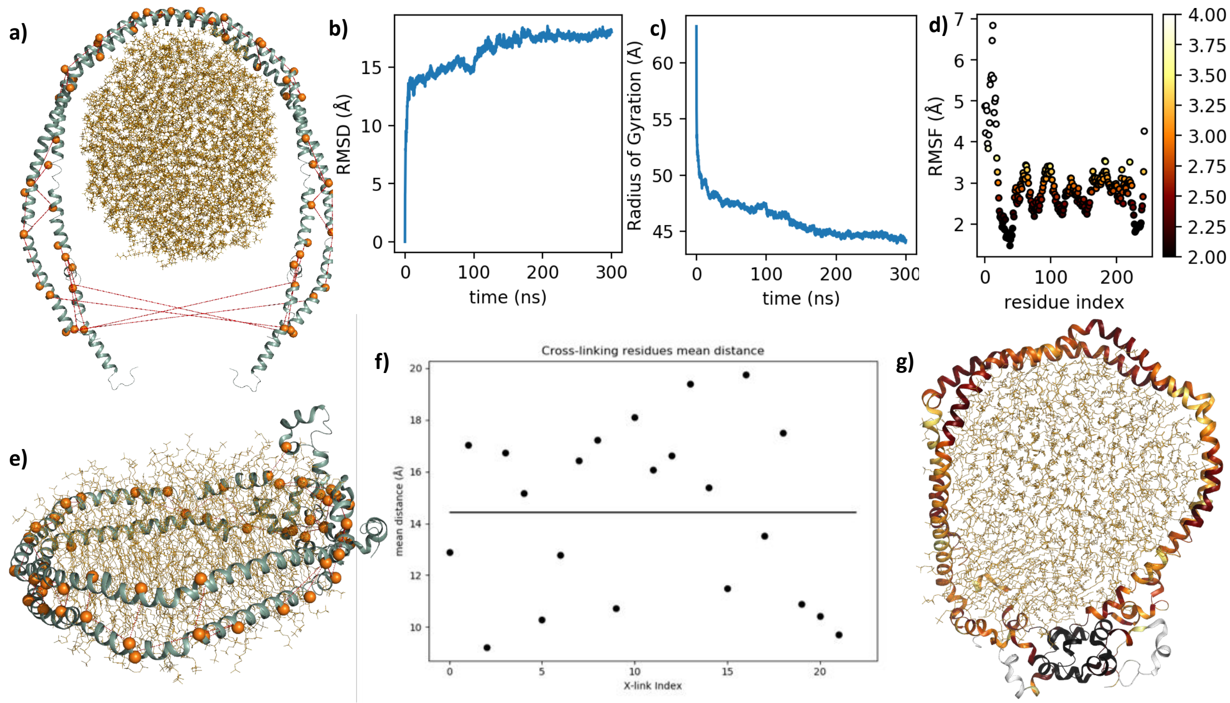

Figure 7 – apoA-I folding. a) 3D structure of raw apoA-I model at t = 0 ns, spheres and dashed lines represent cross-linking atoms; b) RMSD plot; c) Radius of Gyration; d) RMSF plot; e) apoA-I model at t = 100 ns (before the removal of distance restraints), spheres and dashed lines represent cross-linking atoms; f) Restrained atom pairs mean distance after constraints removal. g) model at t = 300 ns, ribbon representation is color-coded on RMSF (d).

According to root-mean-square fluctuation (RMSF) measures, the most mobile apoA-I residues are within the extremities of the N- and C-termini of both chains; while the C-terminus mobility is comparable with a common *end effect*, the increased N-terminus RMSF seems a characteristic feature also described by Jones et al. (2011) (73). However, residues 22–43 and 225–237 folded in a globular structure stabilized by strong electrostatic interactions: hydrogen bonds Arg27-Glu235/Glu234 (existing for 95.6 % of the simulation time), Gly26-Ser231 (58.9 %), Asn43-Gly39 (53.1 %), salt bridges Glu34-Lys238/Lys239 (78.8 % and 76.8 %), Glu234-Lys23/Arg27 (78.6 % and 74.0 %). (Figure 7d). The RMSF analysis also highlighted other mobile domains in apoA-I helical structure: mobile residues 102–111 (H4), 161–169 (H6/7) and 205–221 (H8–H10) formed solvent-exposed bulges with reduced interactions with the lipid core; the elevated mobility of these regions has been previously established by limited proteolysis experiments (74), which have identified cleavage sites to be in positions compatible with our findings. Moreover, as proposed by Wu et al. (2007) (58), the mobility of these regions may be relevant for LCAT recognition. The poorly folded secondary structure encompassing these regions is compliant with observations from Sevugan Chetty et al. (2012) (75), who measured a low stability for the central amphipathic helices, indicating that these residues may be in a dynamic *unfolding and refolding* state. Another notable structural feature of this model is the formation of a tunnel in apoA-I chains in correspondence with residues 121–143 (H5) (Figure 8b). This particular feature has been already observed in a previous computational experiment performed by Jones et al. (2009) (76), where the authors suggest that this *tunnel* may be involved in the *presentation* of substrates to LCAT.

A computational study from Rocco et al. (2010) (77) compared the alignment of adjacent residues (143–165, H6) in natural apoA-I mutants apoA-I_{Milano} and apoA-I_{Paris}, showing that the misalignment of helices 5 and 6 due to a disulfide bridge (Cys173) in apoA-I_{Milano} mutant significantly reduces LCAT activation compared to apoA-I_{Paris}, where the antiparallel 5/5 organization is preserved, but the suboptimal LCAT activation of this latter mutant is likely due to Cys151 disulfide bond falling within a probable LCAT recognition site.

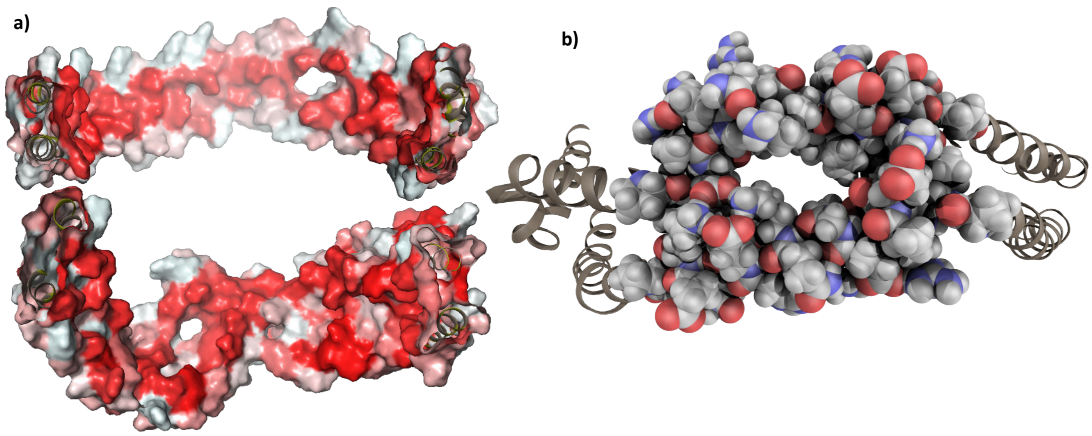

Figure 8 apoA-I structural features. a) Split view of apoA-I inner hydrophobic surfaces (red scale), viewed from the inside of the lipoprotein, central helices (above), termini (below); b) Van der Waal spheres view of the H5 tunnel located between residues 121–143 of apoA-I.

4.2 Assessing LCAT *lid* dynamics

We then moved on the evaluation of published LCAT structures resolved by X-ray crystallography and chose to consider 5TXF and 5BV7 as the two most representative conformations: indeed, these two crystals mainly differ by the arrangement of the *lid-loop* (residues 225–248), a key domain that regulates substrates active site accessibility (13).

While LCAT 5TXF (*closed*) structure formed crystals with an homotetrameric protein organization, 5BV7 (*open*) was crystallized in complex with an agonist antibody that enhances LCAT phospholipasic activity on soluble substrates. Although this may suggest that 5BV7 depicts LCAT in its *active* conformation, the reported *open* conformation of the lid may be artificial; in fact, a visual inspection of the surrounding crystal mates reveals that the first C-terminus residues of the adjacent structure reached into LCAT active site, forcing a wide-open conformation of the lid, as also discussed by Manthei et al. (2017) (13).

To test the hypothesis that the lid-loop conformation in structure 5BV7 depends on the presence of the agonist antibody, we set up two 50 ns MD simulations of 5BV7 LCAT, with and without the co-crystallized antibody fragment. The MD trajectory analyses pointed out that the *Fab-bound* LCAT simulation is the most stable, as shown by the constant RMSD profile (Figure 9a); however, residues with the highest ΔRMSF between the two simulations — that is, residues that account for the highest changes in the *Fab-free* LCAT simulation — are located within LCAT β3/αA domain (Figure 9b). This is also the region recognized by the Fab, indicating that the antibody actually stabilizes an otherwise highly mobile domain of LCAT.

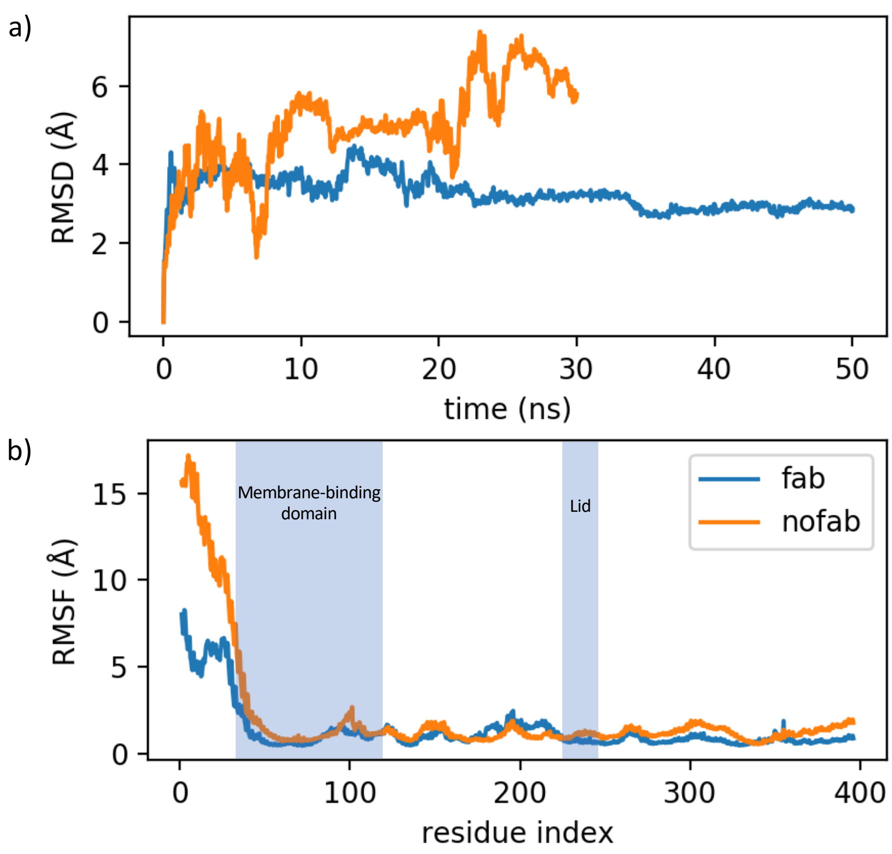

Figure 9 – LCAT MD. Comparison of residues mobility between two LCAT (5BV7) MD simulations with (blue line) and without (orange line) the co-crystallized agonistic antibody: a) RMSD plot; b) RMSF plot, lid loop is comprised between residues 225–250,

within this region RMSFfab − RMSFnofab = −0.075 Å, indicating that there's no significant difference between the mobility of the lid-loop in the two simulations.

These results suggest that the *open* arrangement of the lid observed in 5BV7 is likely not caused by the binding of the antibody fragment to LCAT β3/αA domain, therefore, in our opinion, while not necessarily a crystallographic artefact, 5BV7 is not suitable, without further refinement, to model a physiologically *active* conformation of LCAT. We compared 5BV7 to another open LCAT structure (PDB ID: 6MVD) (78) in complex with a small molecule activator, even if the positioning of the lid loop does not differ significantly from 5BV7 structure; in addition to that, the same crystallographic issues may still persist, in fact, an inspection of the orientation of LCAT proteins within the crystal reveals that LCAT lid loop could be forced in an open position by the surrounding crystal mates. To sample other possible lid-loop conformations we then performed a wtMTD simulation — a sampling technique which allows to describe the energy of the system as a function of reference frames, named collective variables (CVs) (Figure 10a), chosen to track a particular movement —.

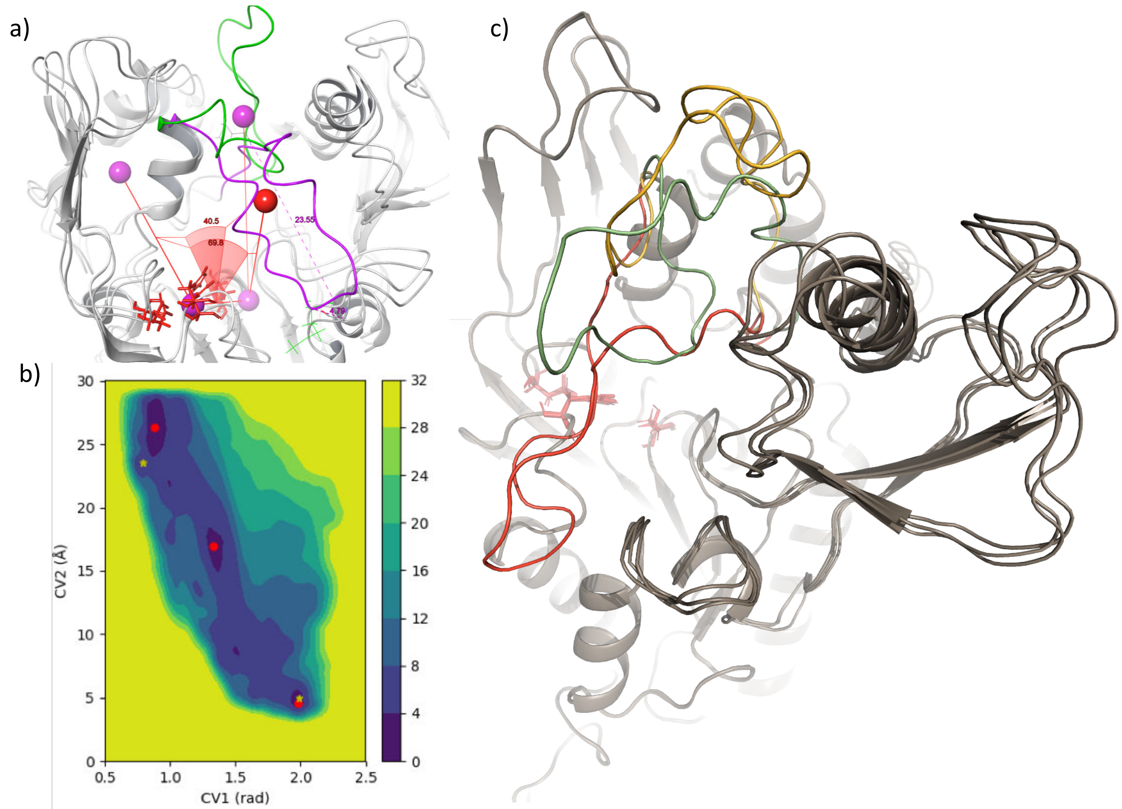

Figure 10 – LCAT wtMTD. a) Collective variables definition: CV1 is the dihedral angle defined by the following atom groups: 1) center of mass of Cap domain 2) center of mass of catalytic triad 3) center of mass of the entire protein except the lid-loop 4) center of mass of the lid-loop; CV2 is the distance between Cα of Met234 and Gly119; b) Free energy surface map as a function of collective variables, red dots indicate relative minima, yellow stars indicate the value of the CVs as in 5TXF and 5BV7 crystallographic structures; c) LCAT structures corresponding to the three relative minima indicated in b), closed (red), intermediate (green), open (yellow).

The free energy surface (FES) generated by the wtMTD displayed three energy wells within 3.5 kcal mol^{-1} from the global minimum (Figure 10b). The structures associated with the minima of such wells correspond to an *open*, *intermediate* and a *closed* LCAT structure (Figure 10c). These results indicate that energy barriers exist along the path that links the open and closed conformations and suggest that external forces may be required for the open-close transition to happen (i.e., the binding to lipoproteins). Intrigued by the identification of a metastable *intermediate* lid loop configuration, we compared it to LPLA2 lid loop (residues 209-231) (PDB ID: 4X90) (79) and found a remarkable similarity between the two structures with respect to the lid loop positioning (RMSD: 16.00 Å) albeit LCAT lid loop lacks the secondary structure element a4 alpha helix described in (79) for LPLA2 and thus exhibits a wider range of motion. It is plausible that the protrusion of the lid loop in the *intermediate* configuration may help in the interaction with lipoproteins, during which LCAT has to interact both with lipids and apoA-I residues and the lid loop has to stretch further to shield the catalytic site. Notably, the lid positioning of the *closed* conformation predicted by the wtMTD almost perfectly overlaps with the lid positioning of the 5TXF crystal structure (RMSD 5.6 Å), conversely, the lid positioning of the predicted *open* conformation shows a greater difference from the one observed in the 5BV7 crystal (RMSD 9.4 Å). Therefore, our predicted *open* LCAT structure may display a more probable and energetically favorable rearrangement of the lid-loop in solution to be used as a starting point for the rHDL-LCAT interactions simulation.

4.3 LCAT binds rHDLs in different positions with varying specificity

To obtain a model of an LCAT::rHDL complex, we employed a protein::protein molecular docking procedure adapted to integrate data gathered from cross-linking experiments and apoA-I mutagenesis studies; the former highlight the residues that are in proximity between LCAT and apoA-I, the latter isolate residues that, when mutated, impaired only LCAT activation while leaving ABCA1-mediated cholesterol efflux unaffected (1,70,76).

We also considered the functional characterization of LCAT glycosylation (80), which showed how the removal of the N-glycan on Asn384 improved LCAT activity on apoA-I-containing proteoliposomes, suggesting that LCAT αF helix of the α/β-hydrolase domain may be directly involved in apoA-I recognition.

Both the *open* and *closed* LCAT structures determined from the wtMTD were used as *ligands* to be docked on the rHDL model after 300 ns MD followed by minimization (for details, please, see Materials and Methods section).

When an unguided docking procedure was applied, most of the generated poses showed non-specific interactions between LCAT β3/αA domain and the phospholipidic surface of the rHDL (data not shown). However, when docking restraints were applied, more specific protein::protein interactions between LCAT and apoA-I could be observed. Experimental data suggest that LCAT may interact with rHDLs in multiple ways, in fact, not all the constraints could be satisfied simultaneously, so different existing models of the LCAT::rHDL complex can be described. We then compared the docking results to apoA-I::LCAT cross-links reported in Manthei et al. (2020) (81), which had not been used to guide the protein::protein docking program, and selected a subset of docking poses that could satisfy multiple interaction hypotheses. Binding poses were also shortlisted on the basis of the proximity between the β3/αA region (membrane-binding domain) and catalytic triad to phospholipids and of the presence of protein-protein interactions between LCAT and apoA-I. The selected binding poses (Figure 11) were then submitted to MD simulations to assess the complex stability over time.

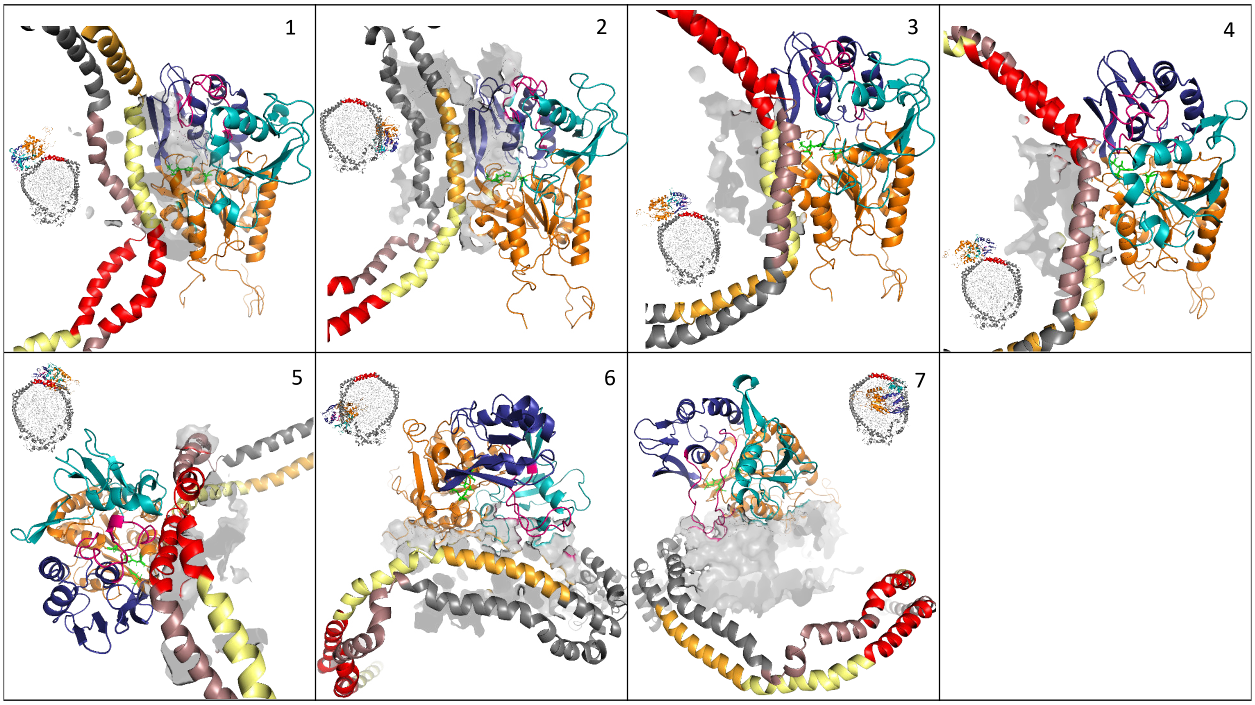

Figure 11 – rHDL::LCAT binding modes. Results of rHDL-LCAT protein-protein docking. Binding poses differ on the basis of the number of constraints satisfied simultaneously. Color code: apoA-I (gray), H4 (pink), H5 (red), H6 (pale yellow), H7 (dark yellow), LCAT α/β-hydrolase fold (orange), lid loop (purple), membrane-binding domain (cyan), cap domain (dark blue), catalytic triad (green sticks), lipids (gray hollow surface). Each figure depicts a small overview of LCAT position with respect to the lipoprotein and a close-up view of the interaction interface. 1) maximized interactions between LCAT α/β-hydrolase domain and apoA-I H6; 2) LCAT Lys240 close to apoA-I Lys182, LCAT α/β-hydrolase domain is close to H6/H7; 3-4) LCAT Lys240 and Ser108 are close to apoA-I Lys140 and Lys118, LCAT α/β-hydrolase domain is contacts apoA-I H5/6; 5) maximized proximity between LCAT Lys240 and Ser108 and apoA-I Lys140 and Lys118 (on both chains), interaction is localized on apoA-I H5; 6) maximized interactions between LCAT and rHDL phospholipid surface, LCAT Lys240 is proximal to apoA-I Lys182 (H7); 7) closed LCAT structure, no protein-protein contacts. Cumulative RMSD between cross-linking atom pairs (Cα): **1** 54.44 Å, **2** 73.89 Å, **3** 53.17 Å, **4** 53.59 Å, **5** 47.49 Å, **6** 70.48 Å, **7** 60.58 Å.

In simulations 2, 3, 4 and 7, the interactions between LCAT and the rHDL are not suitable to maintain the enzyme anchored to the lipoprotein and LCAT drifts away from the complex towards the end of each simulation (Figure 12a). In simulation 2, the cross-linking residue pairs LCAT Lys240 and apoA-I Lys182 (H7) are in proximity and LCAT α/β-hydrolase domain is close to H6/H7; in simulations 3 and 4, the cross-linking residue pairs LCAT Lys240 and Ser108 are close to apoA-I Lys140 and Lys118 (H5/6), while LCAT α/β-hydrolase domain contacts apoA-I H5/6; in simulation 7, no protein-protein interactions form between LCAT and apoA-I and LCAT lid loop is in a closed configuration.

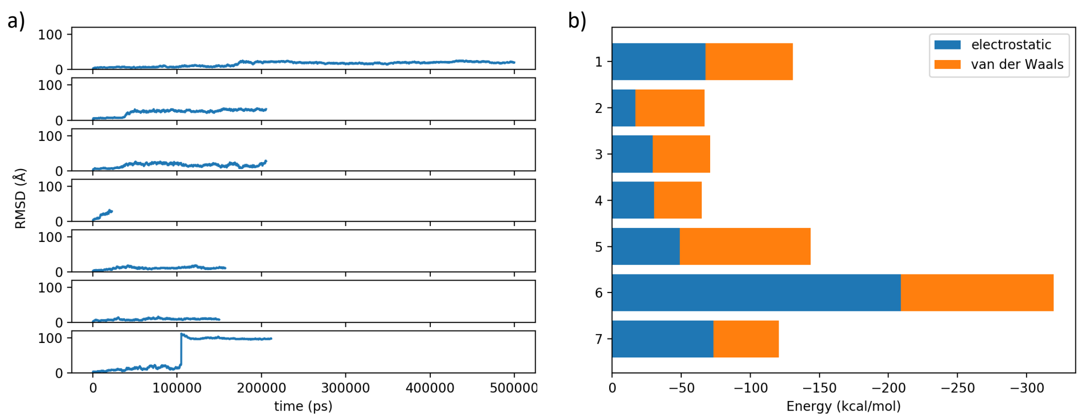

Figure 12 – rHDL::LCAT MD. a) RMSD of LCAT fit on apoA-I; b) Mean LCAT::rHDL binding energy throughout the simulation.

However, in simulations 1, 5 and 6, despite some rearrangements in its positioning, LCAT remains bound to the rHDL with the active site facing the phospholipids. These simulations are characterized by the most negative mean interaction energy values throughout the simulation (Figure 12b), indicating a higher stability of the complexes. Moreover, simulation 5 has the lowest RMSD of distances between residues that can form cross-links (81) (Figure 11, caption). Protein::protein interactions occurring between LCAT and apoA-I are summarized in Table 1.

Table 1 – rHDL::LCAT interactions. The existence of protein-protein interactions with respect to total simulation time is reported. Stars indicate residues associated to FED/FLD (LCAT) or that disrupt LCAT binding/activation when mutated (apoA-I).

rHDL	**LCAT**	**existence %**
Simulation 1		
Hydrogen bonds		
TYR 100	GLN 229	26.59
LYS 118	GLY 374	22.85
ASP 150	ASN 379	21.63
LYS 118	GLN 376	19.92
ASP 103	LYS 240	18.26
ARG 151*	GLN 376	17.01
Salt bridges		
ASP 103*	LYS 240	48.59
LYS 106	ASP 335	12.39
Simulation 5		
Hydrogen bonds		
ARG 123	ASP 335	58.92
GLN 132	ASN 228*	29.44
GLU 139	GLY 119	22.14
LYS 133	LEU 70	22.04
Salt bridges		
ARG 123	ASP 335	62.60
ARG 116	ASP 328	21.23
LYS 140	ASP 113	16.46
Simulation 6		
Hydrogen bonds		
LIP	ARG 244	50.70
LIP	TYR 111*	45.80
LIP	GLU 241	33.62
LIP	HIS 122	32.22
LIP	GLN 126	28.42
LIP	SER 114	27.07
LIP	THR 59	53.54
LIP	ASN 65	25.92
LIP	TYR 111	24.73
LIP	HIS 122	23.78
LIP	ASN 65	22.73
GLU 179	LYS 240	36.11
GLU 183	LYS 238	14.09
Salt bridges		
GLU 179	LYS 240	90.31
GLU 183	LYS 238	61.44
GLU 179	LYS 238	26.47
LIP	CYS 50	21.78

In simulation 1, interactions between LCAT α/β-hydrolase domain and apoA-I H6 are maximized compared to the other systems, while in simulation 5 LCAT binding is localized on apoA-I H5; in simulation 6, protein-protein interactions are limited to few residues in LCAT lid loop and apoA-I H7 in favor of extensive electrostatic interactions between LCAT and the phospholipids. Despite LCAT and N- and C-termini have been described to affect LCAT binding to HDLs (13,82), we could not assign to them a role in the rHDL::LCAT interaction in any of our simulations. This is probably due to the fact that in our systems initial configurations the complex is already formed and LCAT terminal regions may be required during an earlier recognition phase; or else, the simulation time scale was too short to identify LCAT termini interactions with rHDL components given the tested starting configurations.

A possible interpretation of these data is that despite the high tendency of LCAT to form non-specific interactions when close to a lipid interface, specific protein::protein interactions are necessary to stabilize the enzyme on the lipoprotein. Protein::lipid interactions via LCAT β3/αA domain may be required to drive the first recognition then, stronger, specific, protein::protein interactions between apoA-I central helices and LCAT α/β-hydrolase domain are required to properly position LCAT on the lipoprotein and trigger the opening of LCAT lid, with the consequent exposure of the catalytic site (Figure 13).

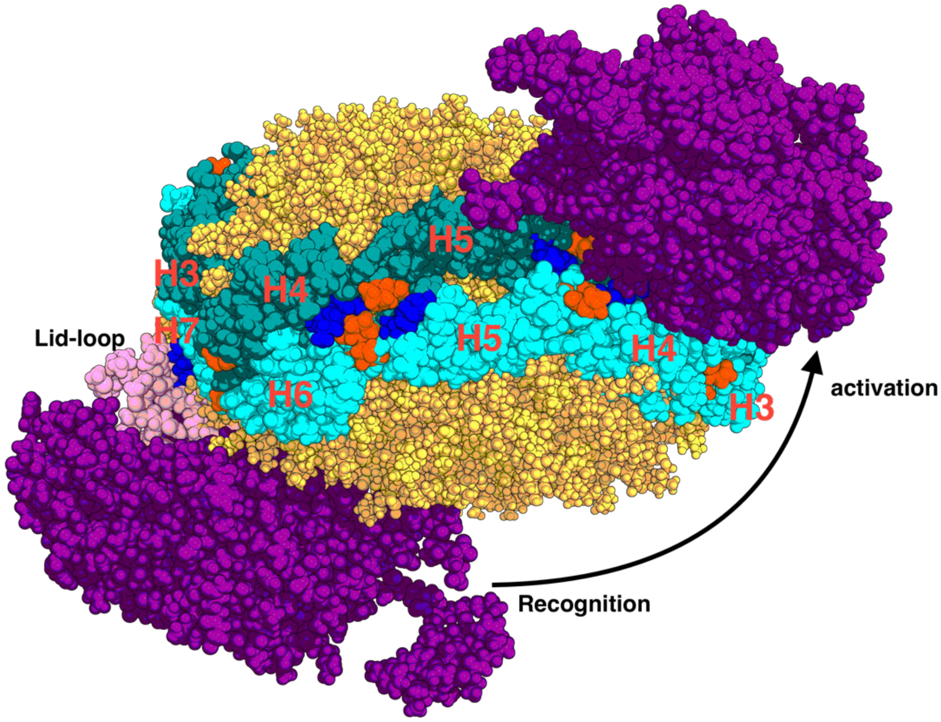

Figure 13 – rHDL::LCAT binding hypothesis. Front view of two complementary rHDL::LCAT binding poses exemplified by simulation 1 (upper-right LCAT position) and simulation 6 (lower-left LCAT position). Both binding modes satisfy complementary cross-linking constraints. As described above, simulation 1 maximizes protein::protein interactions, better explaining, from a theoretical perspective, the *loss-of-function* effects of specific residue mutations. Conversely, although displaying fewer specific protein::protein interactions, simulation 6 has the lowest (better) rHDL::LCAT interaction energy profile and maximizes protein::lipids interactions, moreover, within this binding mode, LCAT active site is closer to its lipidic substrates. We speculate that these two binding modes might coexist in LCAT reaction mechanism and be relevant in distinct phases of substrate (lipoprotein) recognition and enzyme activation. Prolines delimiting apoA-I helices are highlighted orange, cross-linking residues are highlighted blue. LCAT, purple; apoA-I helices, cyan shades.

4.4 LCAT *extracts* phospholipids from the lipoprotein surface

We speculated that LCAT could extract a phospholipid, the first substrate required for the cholesterol trans-esterification mechanism, in the same way as LPLA2 does (79), directly from the surface of the rHDL.

Simulation 6 showed a remarkable LCAT behavior: it *sits* on top of the lipid core and some interactions with apoA-I H7 keep the lid-loop in an open conformation. Because of the binding site shielding operated by the lid-loop, according to this mechanism, substrates would transit directly from the lipid surface to LCAT binding site without exposing their hydrophobic fatty acid chains to the solvent. To simulate the phospholipid *abduction* into LCAT active site, we set up a 50 ns MTD starting from the last frame of simulation 6; a single cv was chosen, represented by the distance between Ser181 hydroxylic group and the carboxylic carbon of the *sn-2* fatty acid chain of the closest phospholipid (Figure 14a). As shown by the FES (Figure 14b), there are no significant energy barriers along the reaction path, indicating that this kind of POPC transition towards LCAT active site might be favorable.

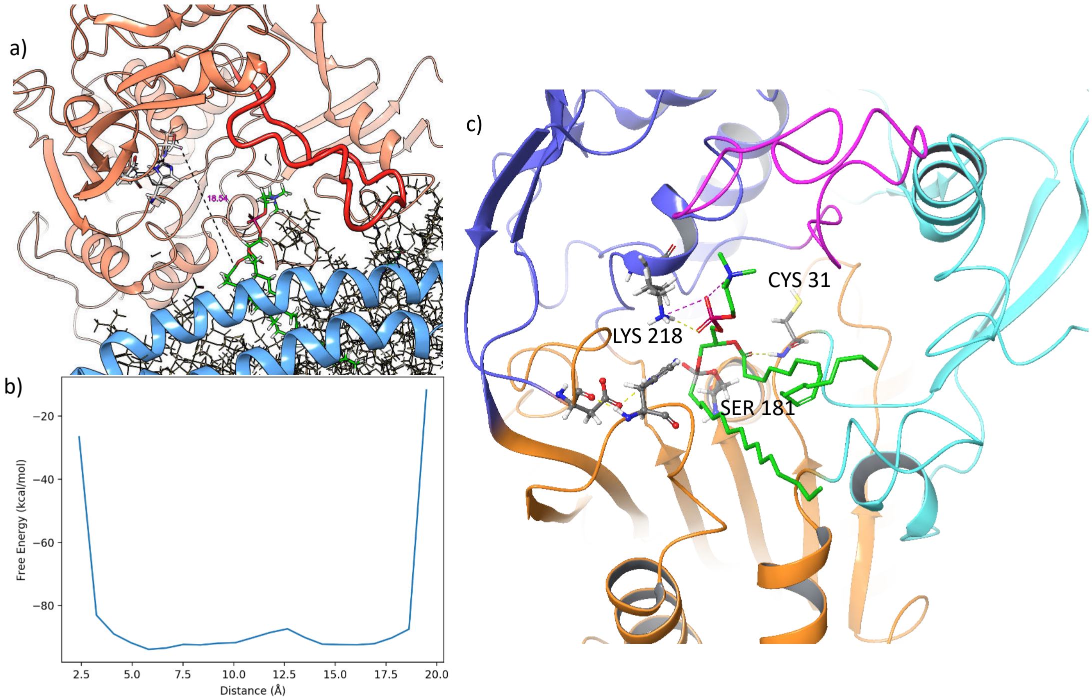

Figure 14 – LCAT acylation. a) definition: distance between Ser181 hydroxyl group and the carboxylic carbon of the sn-2 fatty acid chain of the closest phospholipid; b) FES as function of distance CV, potential grows to infinity as the atoms are pulled too close; c) minimized structure of acylated LCAT, hydrophobicity of binding site is shown as a red surface, salt bridge between Lys218 and phosphate head group as magenta dashed line.

To identify a putative binding mode of the POPC residue within LCAT binding site, the frame corresponding to the lowest CV value was extracted from the wtMTD simulation; and the chemical bonds necessary to obtain the tetrahedral reaction intermediate were manually modified, the acylated enzyme structure was then optimized with a MM/GBSA method (Figure 14c). Notably, during structure optimization of the acyl-enzyme, Lys218 formed a salt bridge with the phospholipid phosphate group; the role of this residue in stabilizing the substrate may explain why its mutation (Lys218Asn) results in FLD syndrome (83).

4.5 Understanding the mechanism-of-action of known LCAT activators

We studied the mechanism of action of two molecules that were proven to be active in restoring the functionality of some LCAT mutants *in vitro*: a piperidinylpyrazolopyridine derivative (78), and a sulfhydryl-reactive molecule, discovered by Amgen, named Compound A (84).

4.5.1 Piperidinylpyrazolopyridine

Part of this study was carried out in collaboration with the pharmaceutical company Daiichi Sankyo, thus, the structure of one of the molecules of interest (the DS compound) could not be disclosed; however, we also studied a similar compound from a recent publication by Manthei et al. (2018) (78).

We aimed at validating the DS compound putative binding site and gain insight into its mechanism of action. We also investigated the effects of mutations on LCAT functionality, stability and their direct effects on DS compound binding affinity.

Evaluation of DS compound binding mode and mechanism of action

DS compound was prepared in order to generate the two possible tautomers that were then docked onto LCAT crystallographic structure (PDB code: 5BV7). The docking algorithm was instructed to use the whole protein as the binding site. Docking poses spanned the entire enzyme, but only two predicted binding sites, shown in Figure 15, had low and comparable energy; one of which is within LCAT active site, the other is in the membrane-binding region, known to be important for lipid and HDL binding. Moreover, another LCAT crystallographic structure (PDB code: 6MVD) (78), depicts the enzyme in complex with an activator drug that is a DS compound conformer, bound in the same region. We exclude the possibility of DS compound binding within LCAT active site, since this would hinder substrates accessibility and inhibit LCAT activity; so, the MBD should be the most plausible binding site, given its importance in lipoprotein recognition and the similarity of DS compound with the co-crystalized drug of the 6MVD LCAT structure.

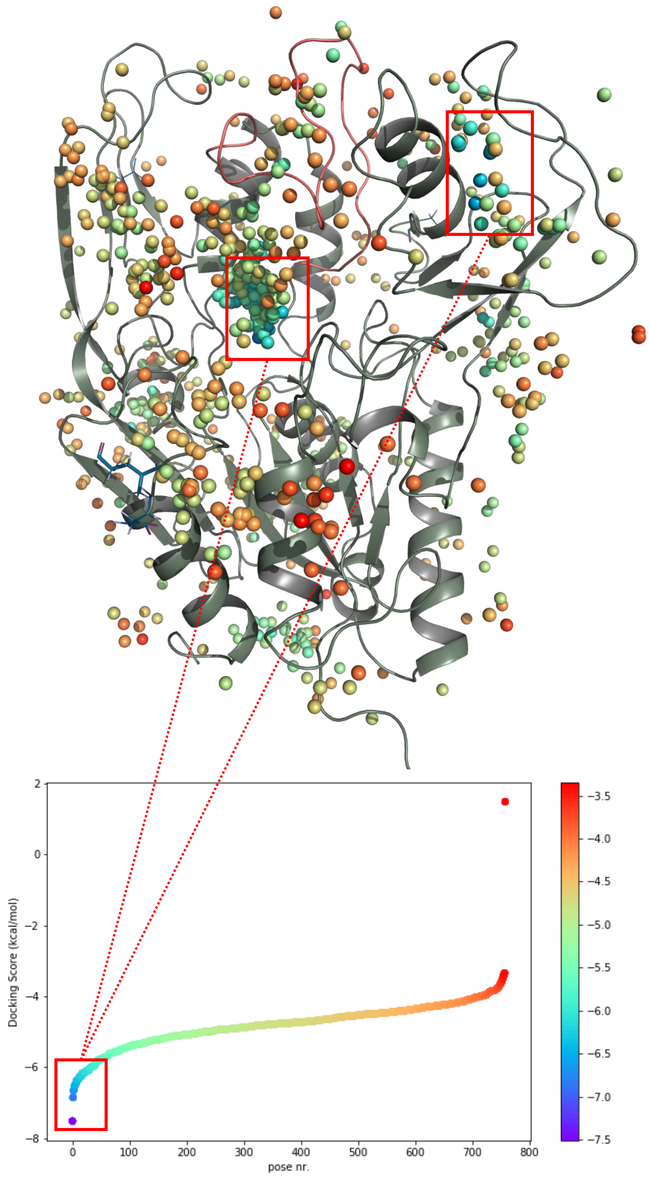

Figure 15 – Binding site identification. Dots represent the center-of-mass positions of DS compound binding poses, colored by docking score values; the two binding sites with lowest energy are highlighted by red boxes and correspond to LCAT binding site (lower) and MBD (upper).

Therefore, we restricted the putative binding site to the MBD region and re-docked the DS compound tautomers on 6MVD LCAT structure. The original co-crystalized activator was also docked for validation purposes (binding free energy -6.807 kcal/mol): the coordinates of the top-scoring predicted binding pose and of the crystallographic one were almost overlapping, with a RMSD of 0.3Å, consequently, we expect the predicted binding poses for DS compound to be accurate. DS compound predicted binding pose was further minimized following a Monte Carlo method. The computed binding free energy is -8.063 kcal/mol, and the ΔG between the two tautomers is 1.697 kcal/mol.

We then performed molecular dynamics simulations to assess the stability of the LCAT::drug complex. We also compared the LCAT:DS-compound (holo) simulation to a simulation of LCAT alone (apo) to highlight structural modifications induced by the binding of SD compound.

The analysis of protein-ligand interactions during the MD simulation highlighted key residues for DS compound binding to LCAT. In particular, persistent hydrogen bonds (> 90% of simulation time) form between DS compound and Asp63, Asn78 and Try51, which also forms a pi-pi interaction with the DS condensed rings, while Leu68 and Cys74 contribute with hydrophobic interactions (Figure 16).

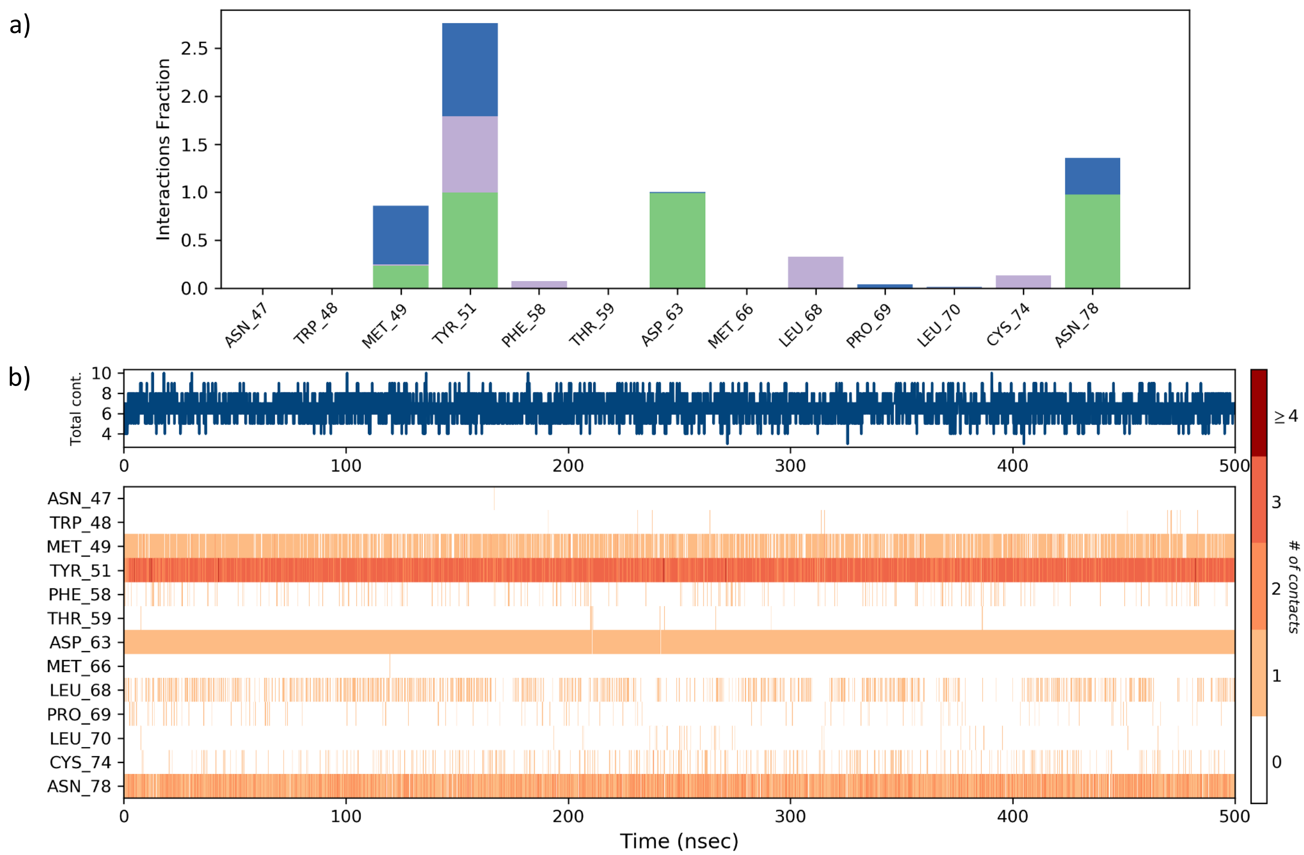

Figure 16 – MD ligand-protein interactions. Residues that interact more than 30% simulation time are reported. a): type of interaction, hydrogen bond (green), hydrophobic (purple), ionic (blue). b) Existence map of interactions.

Two major clusters could be observed with respect to ligand conformations (measured in terms of RMDS) within its binding site, these two states have different interaction energies, in fact, fluctuations in ligand positioning correlate with fluctuations in interaction energies, as shown in Figure 17; the largest cluster (70% of MD frames) has a mean interaction energy of −72.70 kcal/mol, while the other −67.43 kcal/mol. Note that interaction energy values calculated by a force field from an explicit-solvent molecular dynamics simulation are different than the ones generated by docking empirical scoring functions, also because of a different use of implicit/explicit solvation models.

Comparing the mobility of residues of the apo and holo forms of LCAT, while the mobility of DS compound binding pocket remains unaltered, residues 45–47 of the membrane binding domain gain increased mobility; moreover, the lid loop, responsible of regulating the accessibility of substrates to LCAT binding site, is much more stable (in an open conformation) when DS compound is bound to LCAT (Figure 18).

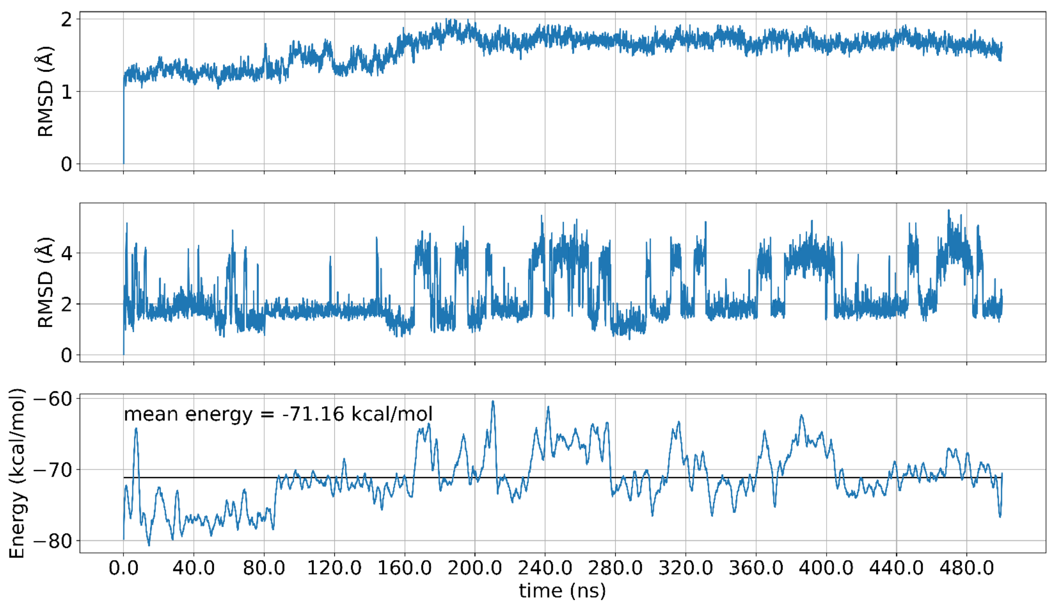

Figure 17 – MD structure analysis. Top, RMSD of LCAT, a plateau indicates reach of a stable conformation; middle, RMSD of SD compound, oscillations between different states can be observed; clustering of ligand conformations reveals that mainly two states exist during MD simulation, one occurring for ~70% of simulation time, with a mean interaction energy of -72.70 kcal/mol, and one occurring for ~30% of simulation time with a mean interaction energy of -67.43 kcal/mol.

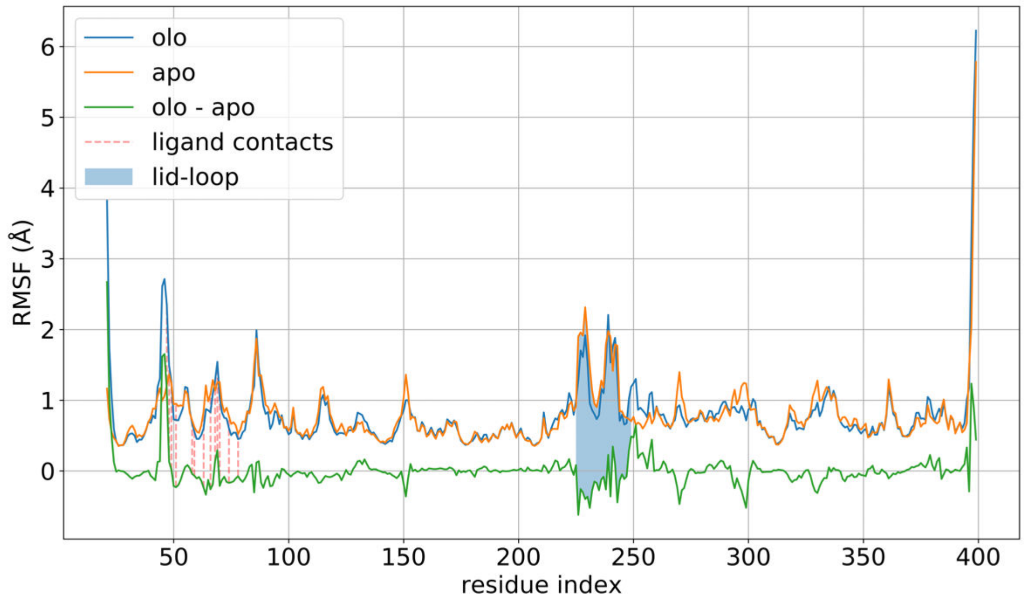

Figure 18 – Comparison between LCAT apo and holo forms. RMSF of LCAT residues; residues interacting with DS compound and the lid loop are highlighted.

*Overall, DS compound activity could be explained by its ability to stabilize the lid loop in an open conformation and by increasing LCAT affinity to lipid membranes by enhancing the hydrophobicity of the MBR region and/or by facilitating its interaction with lipids***.**

Evaluation of the structural impact of reference LCAT mutations

Specified LCAT mutations were introduced on LCAT 6MVD structure, bound to DS compound. This procedure (Prime, Schrodinger) then samples and minimizes the structure of atoms surrounding the mutated residues and computes the variations in ligand affinity and protein stability with respect to the *wild type (wt)* original structure. Results, summarized in Table 2, show clearly that mutations have little to no effect on DS compound binding affinity, but may greatly alter protein stability; in particular, Arg147Trp, Pro254Ser and Ser91Pro/Ala141Thr mutations are predicted to significantly alter LCAT structure.

Table 2 – Residue mutation analysis. Differences in affinity and stability are calculated with respect to the *wt* LCAT.

Residue	Original	Mutated	d Affinity	d Stability (solvated)
91, 141	SER ALA	PRO THR	0.01	12.63
147	ARG	TRP	0.54	58.88
274	THR	ILE	0.00	1.58
372	LEU	ARG	-0.00	-0.26
254	PRO	SER	-0.00	16.30
309	VAL	MET	-0.00	4.26

Figure 19 shows the mapping of reference mutations on the wt LCAT structure; the effects of some mutations can be explained by visual inspection:

- mutation Pro254Ser introduces a hydrophilic residue within a pack of hydrophobic residues in the proximity of the lid loop, likely disrupting LCAT fold. This may explain why the resulting mutant is unable to be rescued by DS compound (data not shown).
- Mutation Arg147Trp is also predicted to largely impact on LCAT structure, and its position is in a region known to impact substrate (phospholipids) binding.
- Mutation Leu372Arg does not seem to affect LCAT folding, however, it falls in a region likely involved in Apo-AI recognition. The effect of this mutation may be well compensated by DS compound ability to enhance LCAT binding to lipids.
- Thr274Ile and Val309Met are predicted to have little to no effect on LCAT structure alterations, the SIFT webserver was also used to corroborate these results (mutations are TOLERATED with a score of 0.10 and 0.35 respectively). Given that Thr274 and Val309 are far from the active site or the putative LCAT::lipoprotein interaction interface, and that protein stability is not affected by these mutations, our results suggest that they may indirectly affect lipoprotein recognition.

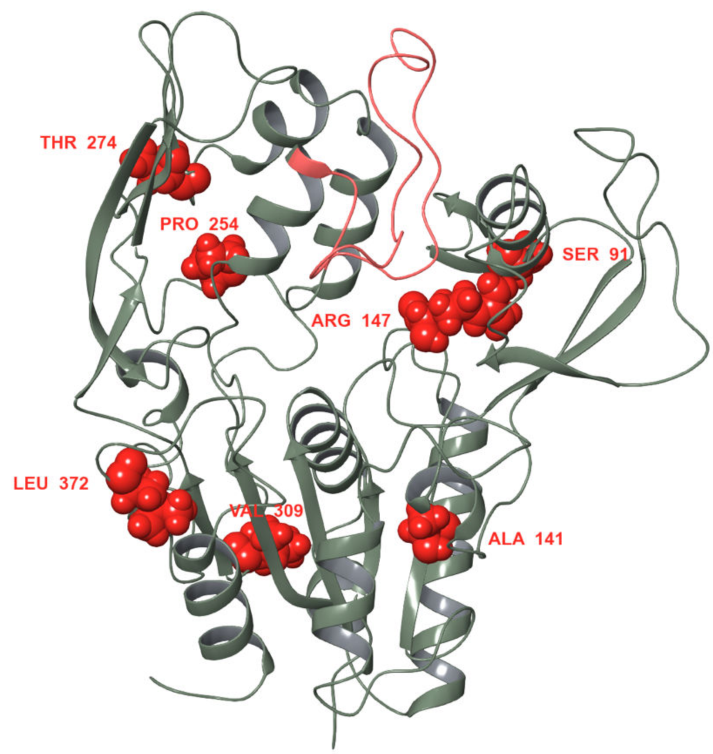

Figure 19 – Reference mutations mapping to LCAT structure. Residues at positions affected by reference mutations are represented with red spheres, LCAT *lid* loop is highlighted in red.

4.5.2 LCAT MBD allosteric activators enhance membrane affinity

Part of the activity of the piperidinylpyrazolopyridine allosteric LCAT activators could be explained by compounds ability to increase LCAT membrane affinity. Indeed, as discussed by Manthei et al. (2018) (78), active piperidinylpyrazolopyridine derivatives expand LCAT MBD hydrophobic surface through a terminal solvent-exposed hydrophobic moiety.

We tested the hypothesis that this class of compounds could enhance LCAT binding to lipids by simulating LCAT attachment and detachment from a lipid bilayer (20:1 POPC:CHOL) in the presence or absence of LCAT 6MVD co-crystalized ligand with steered molecular dynamics (sMD) simulation. We show that the force required to *pull* LCAT away from the membrane is greater in the presence of the allosteric ligand compared to the *apo* LCAT (Figure 20a). Moreover, we observed that ligands in this position may enhance lipid-binding cooperatively with Trp48, a residue that was proved to be important for binding to HDLs (13) (Figure 20b). In fact, we have found that the allosteric ligand could not only interact with lipid molecules, but it may also affect the mobility of Trp48, possibly forcing it to protrude more from LCAT MBD.

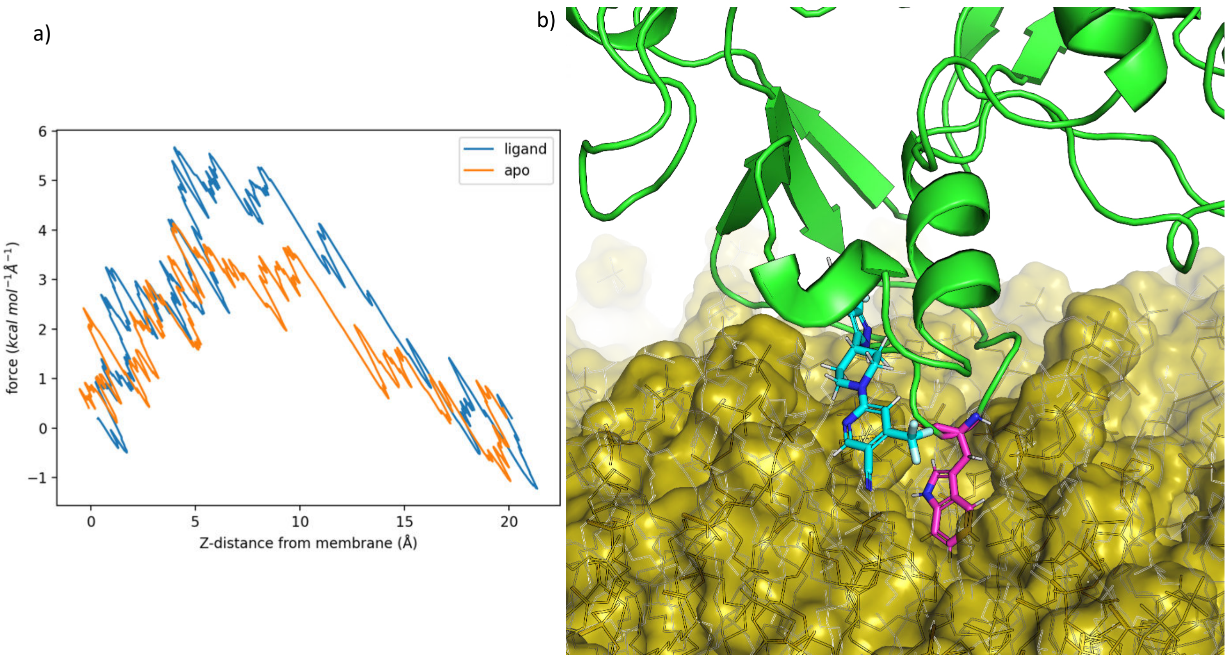

Figure 20 – Effect of ligands on LCAT::membrane detachment. a) Running average force profile of LCAT::membrane detachment measured with steered MD in the presence or absence of the allosteric LCAT activator described by Manthei et al in (78). Z-distance is calculated for LCAT center-of-mass with respect to its starting configuration at time $t = 0$. b) Snapshot of the starting configuration: the allosteric ligand and Trp48 are buried within the membrane; lipids, yellow surfaces; ligand, cyan, Trp48, magenta; LCAT, green ribbons.

4.5.3 Compound A

Compound A [3-(5-(ethylthio)-1,3,4-thiadiazol-2-ylthio)pyrazine-2-carbonitrile)], was discovered by Amgen in a high-throughput screen (84). Freeman et al. (2017) (85) tested Compound A activity on human plasma, showing that it was able to increase LCAT activity in a subset of LCAT mutations to levels comparable to FLD heterozygotes. They also demonstrated that Compound A activity is due to acylation of Cys31 within LCAT substrate binding site, increasing LCAT binding site hydrophobicity, thus improving substrate recognition. However, our MD simulations showed that LCAT becomes less stable when covalently bound to the drug (Figure 21a): the lid loop and membrane-binding domain gain increase mobility (Figure 21b), possibly affecting lipoprotein recognition in addition to substrate binding.

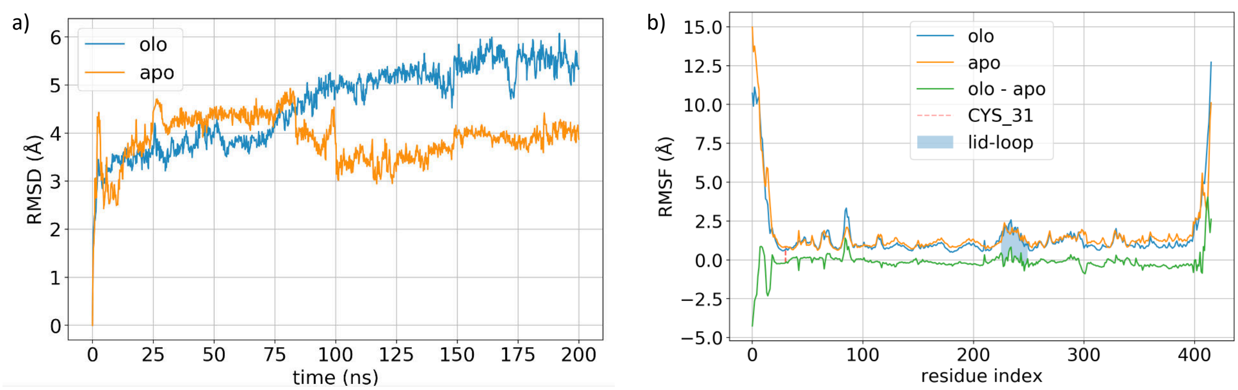

Figure 21 – LCAT::Compound MD analysis. a) RMSD profile, compound A-bound LCAT is significantly less stable than the apo-protein. b) RMSF profile, lid-loop, highlighted, is slightly more mobile when compound A is present within LCAT active site.

4.6 Preliminary investigation on novel compounds

As discussed by Freeman et al. (2017) (85), development of alkylating LCAT compound A-based activators is challenging, as they will have to be electrophiles that selectively react only with Cys31 and not with the active site serine residue; another limitation of these compounds, shared by many drugs that target sulfhydryl groups, is the lack of specificity, as they may react with glutathione or reactive cysteines on other proteins (86). For these reasons, focusing the attention on MBD-binding compounds based on (85) could be more beneficial to finding molecules that better translate into new drugs for FLD treatment.

We screened a library of ~100,000 lead-like compounds on LCAT membrane-binding domain. We found molecules with a better predicted binding affinity sharing a similar scaffold and chemical features (aromatic and pyrazole rings) (Figure 22).

In the future, these molecules could be further optimized with computational medicinal chemistry, providing lead-like LCAT modulators potentially active at lower concentrations, with less off-target effects and higher efficiency on different LCAT mutants.

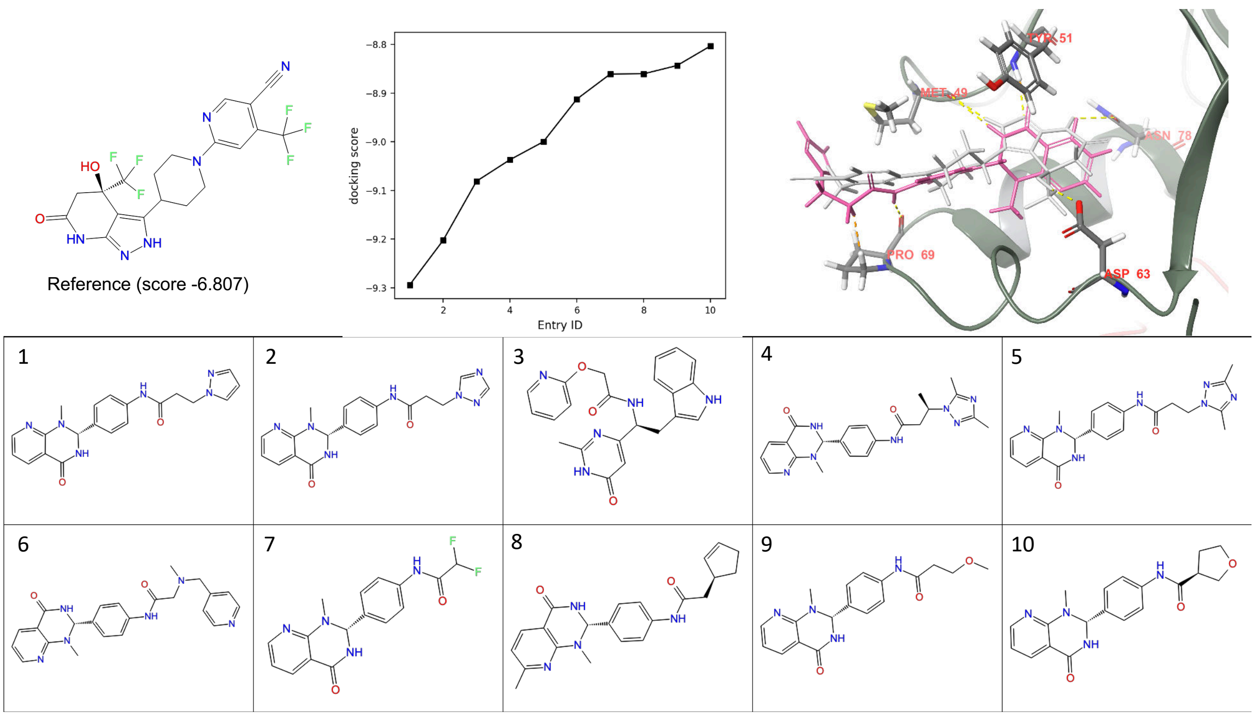

Figure 22 – LCAT virtual screening. The 10 top-scoring molecules of the Asinex "Elite Sinergy" library are reported along with their docking score (which correlates with binding free energy). The reference compound co-crystalized with LCAT 6MVD is also shown (top right). Top-right, a close-up of the binding site showing the binding mode of the reference compound (pink) and the top-scoring molecule (#1) (white); conserved hydrogen bonds are shown with dashed lines (yellow) between the ligands and residues, Met49, Tyr51, Asp63, Pro69 and Asn78.

5 FINAL CONCLUSIONS

We generated an all-atom model of a reconstituted HDL making use of restrained MD by integrating experimental cross-linking and crystallographic data. The resulting model satisfied other biochemical observations, such as particle size, α-helicity content and tryptophan solvent accessibility; high-mobility regions at N- and C-termini and within apoA-I central helices were also consistent with HDX and limited proteolysis experiments. To our knowledge, this is the first time that a full-atom structure of lipid-bound apoA-I was generated from crystallographic data on the delipidated protein; the integration of cross-linking experiments into a restrained MD simulation was aimed at minimizing the biases related to the chosen starting configuration for the system, by allowing apoA-I to smoothly *fold* and rearrange itself around the lipid core instead of constraining its structure into circular double-helix belt. This approach also allowed us to deal with apoA-I N-termini without the need to guess their structure or truncate the protein sequence.

We studied and compared published LCAT crystallographic structures and an energetically stable LCAT structure in an open (active) conformation was obtained refining the experimental data with wtMTD simulations. Notably, our LCAT MD simulations show that the lid loop arrangement is decoupled from the dynamics of the membrane-binding domain, suggesting that specific interactions with apoA-I are required to stabilize an *open* configuration.

The generated rHDL model was used as a receptor to study LCAT recognition and activation mechanism. We used an integrative approach to build several models of rHDL::LCAT interactions combining data from mutagenesis and cross-linking experiments through molecular docking and then tested the dynamic behavior and the stability of the generated models with MD simulations.

Our findings on the LCAT::rHDL are complementary with the model proposed by Manthei et al. (2020) (81), where the authors integrated EM and cross-link/MS analyses to conclude that LCAT preferentially binds to helices 4/6 of apoA-I on the edge of the lipoprotein. The use of MD simulations to assess the stability of several interaction models allowed us to corroborate the importance of LCAT α/β-hydrolase fold and apoA-I helices 4-7 for their molecular recognition mechanism. However, we also observed that other binding modes involving LCAT membrane-binding domain are stable and could be functional to the enzyme activity. Castelijn et al. (87) simulated the binding of LCAT to a lipid bilayer coupling their MD simulations with free-energy calculations methods; our results supports their hypothesis that the main driver of the rHDL::LCAT recognition mechanism is the interaction between LCAT membrane-binding domain (β3/αA) and the lipid surface. As exemplified by simulation 6 described in this manuscript, we showed how less specific protein::lipid interactions indeed contribute to LCAT binding on the lipoprotein, and we further described the specific protein-protein interactions that are required to drive the opening of LCAT lid. Elaborating further on this interaction model, we then simulated the first step of LCAT reaction mechanism, showing that the extraction of a phospholipid from the rHDL lipid core occurs without having to cross significant energy barriers, resulting in the subsequent acylation of the enzyme. We speculated that two complementary binding modes characterized by non-specific LCAT::lipids or specific LCAT::apoA-I interactions could be subsequent steps of the same LCAT reaction mechanism needed first for substrate recognition and then activation of the enzyme. Unfortunately, the short timescale imposed by the state of the art of classical molecular dynamics simulations does not allow us to look for large-scale transitions in the binding mode of LCAT nor to simulate the full reaction cycle of lipoprotein-binding, activation and catalysis.

We hope this work can help to support and pull together the accumulated literature on the subject of LCAT and (r)HDL interactions, as well as to address the focus of future research, that should be aimed at clarifying the functional role and the transition dynamics between the multiple binding modes that LCAT exhibits with respect to apoA-I-containing lipoproteins.

We also investigated the mechanism of action of two classes of known LCAT activators, focusing our attention to piperidinylpyrazolopyridines derivatives that target LCAT membrane binding domain. We show that the activity of this latter class of compounds can be explained by the stabilization of the lid loop in an open conformation and by the increase of LCAT affinity to lipid membranes. The hydrophobic moiety of the ligands that protrudes from LCAT MBD strengthen membrane binding by directly interacting with lipids, however, we speculate that the binding of the allosteric activator could also affect the structure of residues known to be important for membrane recognition (such as Trp48 (13)), allowing them to better interact themselves with lipids.

Based on our model of the LCAT::rHDL interaction, these compounds could be effective in the first phase of rHDL recognition, that is binding to the lipoprotein, and they are not predicted to favor specific LCAT-apolipoprotein interactions that are then required to activate the enzyme. However, based on *in silico* mutagenesis analyses, these allosteric activators could still efficiently rescue some naturally occurring FLD LCAT mutants.

High throughput *virtual* screening of lead-like compounds has yielded molecules physiochemically similar to the reference activator (78) with a higher predicted binding affinity to LCAT MBD. Further studies are needed to predict the activity of these compounds and subsequently optimize their design with computational medicinal chemistry. Our next goal is to provide lead-like LCAT modulators ready to be tested *in vitro* and *in vivo,* that are potentially active at lower concentrations and with higher efficiency on different LCAT mutants to be used in the treatment of LCAT deficiency syndromes and cardiovascular diseases.

REFERENCES

1. Jonas A. Lecithin cholesterol acyltransferase. Biochim Biophys Acta - Mol Cell Biol Lipids [Internet]. 2000;1529(1–3):245–56. Available from: http://www.sciencedirect.com/science/article/B6VNN-41T1FT7-R/1/950547bd5442395f5bec77aea588c6ce%5Cnpapers2://publication/uuid/51034E11-DC3C-4412-B527-F3075889B251

2. Asztalos BF, Schaefer EJ, Horvath K V, Yamashita S, Miller M, Franceschini G, et al. Role of LCAT in HDL remodeling: investigation of LCAT deficiency states. J Lipid Res [Internet]. 2007 Mar;48(3):592–9. Available from: http://www.jlr.org/cgi/reprint/48/3/592%5Cnhttp://dx.doi.org/10.1194/jlr.M600403-JLR200%5Cnhttp://www.ncbi.nlm.nih.gov/pubmed/?term=17183024http://www.ncbi.nlm.nih.gov/pubmed/?term=17183024http://www.ncbi.nlm.nih.gov/pubmed/?term=17183024http://www.ncbi.n

3. Ossoli A, Pavanello C, Calabresi L, Paoletti CEG. High-Density Lipoprotein, Lecithin: Cholesterol Acyltransferase, and Atherosclerosis. Endocrinol Metab. 2016;31:223–9.

4. Calabresi L, Gomaraschi M, Villa B, Omoboni L, Dmitrieff C, Franceschini G. Elevated soluble cellular adhesion molecules in subjects with low HDL-cholesterol. Arterioscler Thromb Vasc Biol. 2002;22(4):656–61.

5. Saeedi R, Li M, Frohlich J. A review on lecithin:cholesterol acyltransferase deficiency. Clin Biochem [Internet]. 2015;48(7–8):472–5. Available from: http://www.sciencedirect.com/science/article/pii/S0009912014006493

6. Ossoli A, Neufeld EB, Thacker SG, Vaisman B, Pryor M, Freeman LA, et al. Lipoprotein X Causes Renal Disease in LCAT Deficiency. PLoS One [Internet]. 2016;11(2):e0150083. Available from: http://www.ncbi.nlm.nih.gov/pubmed/26919698

7. AZOULAY M, HENRY I, TATA F, WEIL D, GRZESCHIK KH, CHAVES ME, et al. The structural gene for lecithin:cholesterol acyl transferase (LCAT) maps to 16q22. Ann Hum Genet. 1987 May;51(2):129–36.

8. Warden CH, Langner CA, Gordon JI, Taylor BA, McLean JW, Lusis AJ. Tissue-specific expression, developmental regulation, and chromosomal mapping of the lecithin: cholesterol acyltransferase gene. Evidence for expression in brain and testes as well as liver. J Biol Chem. 1989 Dec;264(36):21573–81.

9. Piper DE, Romanow WG, Gunawardane RN, Fordstrom P, Masterman S, Pan O, et al. The high-resolution crystal structure of human LCAT. J Lipid Res [Internet]. 2015;56(9):1711–9. Available from: http://www.jlr.org/lookup/doi/10.1194/jlr.M059873

10. Sensi C, Simonelli S, Zanotti I, Tedeschi G, Lusardi G, Franceschini G, et al. Distant homology modeling of LCAT and its validation through in silico targeting and in vitro and in vivo assays. PLoS One [Internet]. 2014;9(4):e95044. Available from: http://www.ncbi.nlm.nih.gov/pubmed/24736652

11. J.P. S, M.K. J, A. C, S.P. T. A robust all-atom model for LCAT generated by homology modeling. J Lipid Res [Internet]. 2015;56(3):620–34. Available from:

http://www.embase.com/search/results?subaction=viewrecord&from=export&id=L602911364%5Cnhttp://dx.doi.org/10.1194/jlr.M056382%5Cnhttp://rd8hp6du2b.search.serialssolutions.com?sid=EMBASE&issn=15397262&id=doi:10.1194/jlr.M056382&atitle=A+robust+all-atom+mode

12. Adimoolam S, Jonas A. Identification of a domain of lecithin-cholesterol acyltransferase that is involved in interfacial recognition. Biochem Biophys Res Commun. 1997;232(3):783–7.

13. Manthei KA, Ahn J, Glukhova A, Yuan W, Larkin C, Manett TD, et al. A retractable lid in lecithin:cholesterol acyltransferase provides a structural mechanism for activation by apolipoprotein A-I. J Biol Chem [Internet]. 2017;(Ldl):jbc.M117.802736. Available from: http://www.jbc.org/lookup/doi/10.1074/jbc.M117.802736

14. Liu M, Subramanian VS, Subbaiah P V. Modulation of the positional specificity of lecithin-cholesterol acyltransferase by the acyl group composition of its phosphatidylcholine substrate: Role of the sn-1-acyl group. Biochemistry. 1998;

15. Subbaiah P V., Monshizadegan H. Substrate specificity of human plasma lecithin-cholesterol acyltransferase towards molecular species of phosphatidylcholine in native plasma. Biochim Biophys Acta - Lipids Lipid Metab. 1988 Dec;963(3):445–55.

16. Parks JS, Gebre AK. Long-chain polyunsaturated fatty acids in the sn-2 position of phosphatidylcholine decrease the stability of recombinant high density lipoprotein apolipoprotein A-I and the activation energy of the lecithin:cholesterol acyltransferase reaction. J Lipid Res. 1997 Feb;38(2):266–75.

17. Nakamura Y, Kotite L, Gan Y, Spencer TA, Fielding CJ, Fielding PE. Molecular Mechanism of Reverse Cholesterol Transport: Reaction of Pre-β-Migrating High-Density Lipoprotein with Plasma Lecithin/Cholesterol Acyltransferase †. Biochemistry. 2004 Nov;43(46):14811–20.

18. Chen C-H, Albers JJ. Distribution of lecithin-cholesterol acyltransferase (LCAT) in human plasma lipoprotein fractions. Evidence for the association of active LCAT with low density lipoproteins. Biochem Biophys Res Commun. 1982 Aug;107(3):1091–6.

19. Kosek AB, Durbin D, Jonas A. Binding Affinity and Reactivity of Lecithin Cholesterol Acyltransferase with Native Lipoproteins. Biochem Biophys Res Commun. 1999 May;258(3):548–51.

20. Chang T-Y, Li B-L, Chang CCY, Urano Y. Acyl-coenzyme A:cholesterol acyltransferases. Am J Physiol Metab. 2009 Jul;297(1):E1–9.

21. Norum KR, Gjone E. Familial serum-cholesterol esterification failure. A new inborn error of metabolism. Biochim Biophys Acta - Lipids Lipid Metab. 1967 Dec;144(3):698–700.

22. Oldoni F, Sinke RJ, Kuivenhoven JA. Mendelian Disorders of High-Density Lipoprotein Metabolism. Circ Res. 2014 Jan;114(1):124–42.

23. Calabresi L, Pisciotta L, Costantin A, Frigerio I, Eberini I, Alessandrini P, et al. The Molecular Basis of Lecithin:Cholesterol Acyltransferase Deficiency Syndromes. Arterioscler Thromb Vasc Biol. 2005 Sep;25(9):1972–8.

24. Calabresi L, Baldassarre D, Castelnuovo S, Conca P, Bocchi L, Candini C, et al. Functional lecithin: cholesterol acyltransferase is not required for efficient atheroprotection in humans.

Circulation [Internet]. 2009 Aug 18;120(7):628–35. Available from: http://www.ncbi.nlm.nih.gov/pubmed/19687369

25. Boscutti G, Calabresi L, Pizzolitto S, Boer E, Bosco M, Mattei PL, et al. [LCAT deficiency: a nephrological diagnosis]. G Ital Nefrol. 28(4):369–82.

26. Panescu V. Recurrence of lecithin cholesterol acyltransferase deficiency after kidney transplantation. Nephrol Dial Transplant. 1997 Nov;12(11):2430–2.

27. Rousset X, Vaisman B, Auerbach B, Krause BR, Homan R, Stonik J, et al. Effect of Recombinant Human Lecithin Cholesterol Acyltransferase Infusion on Lipoprotein Metabolism in Mice. J Pharmacol Exp Ther. 2010 Oct;335(1):140–8.

28. Shamburek RD, Bakker-Arkema R, Auerbach BJ, Krause BR, Homan R, Amar MJ, et al. Familial lecithin:cholesterol acyltransferase deficiency: First-in-human treatment with enzyme replacement. J Clin Lipidol. 2016;10(2):356–67.

29. Shamburek RD, Bakker-Arkema R, Shamburek AM, Freeman LA, Amar MJ, Auerbach B, et al. Safety and Tolerability of ACP-501, a Recombinant Human Lecithin:Cholesterol Acyltransferase, in a Phase 1 Single-Dose Escalation Study. Circ Res. 2016 Jan;118(1):73–82.

30. Chisholm JW, Burleson ER, Shelness GS, Parks JS. ApoA-I secretion from HepG2 cells: evidence for the secretion of both lipid-poor apoA-I and intracellularly assembled nascent HDL. J Lipid Res. 2002 Jan;43(1):36–44.

31. Ikewaki K, Zech LA, Brewer HB, Rader DJ. ApoA-II kinetics in humans using endogenous labeling with stable isotopes: slower turnover of apoA-II compared with the exogenous radiotracer method. J Lipid Res. 1996 Feb;37(2):399–407.

32. Edelstein C, Gordon JI, Toscas K, Sims HF, Strauss AW, Scanu AM. In vitro conversion of proapoprotein A-I to apoprotein A-I. Partial characterization of an extracellular enzyme activity. J Biol Chem. 1983 Oct;258(19):11430–3.

33. Tsujita M, Wu C-A, Abe-Dohmae S, Usui S, Okazaki M, Yokoyama S. On the hepatic mechanism of HDL assembly by the ABCA1/apoA-I pathway. J Lipid Res. 2005 Jan;46(1):154–62.

34. Gu F, Jones MK, Chen J, Patterson JC, Catte A, Jerome WG, et al. Structures of discoidal high density lipoproteins: A combined computational-experimental approach. J Biol Chem. 2010;285(7):4652–65.

35. Heinecke JW. The HDL proteome: a marker–and perhaps mediator–of coronary artery disease. J Lipid Res. 2009;50:S167–71.

36. Zechner R, Dieplinger H, Steyrer E, Groener J, Calvert D, Kostner GM. In vitro formation of HDL-2 from HDL-3 and triacylglycerol-rich lipoproteins by the action of lecithin: cholesterol acyltransferase and cholesterol ester transfer protein. Biochim Biophys Acta - Lipids Lipid Metab. 1987 Mar;918(1):27–35.

37. Klerkx AHEM, Harchaoui K El, van der Steeg WA, Boekholdt SM, Stroes ESG, Kastelein JJP, et al. Cholesteryl Ester Transfer Protein (CETP) Inhibition Beyond Raising High-Density Lipoprotein Cholesterol Levels. Arterioscler Thromb Vasc Biol. 2006 Apr;26(4):706–15.

38. Clay MA, Newnham HH, Forte TM, Barter PI. Cholesteryl ester transfer protein and hepatic lipase activity promote shedding of apo A-I from HDL and subsequent formation of discoidal HDL. Biochim Biophys Acta - Lipids Lipid Metab. 1992 Feb;1124(1):52–8.

39. Moestrup SK, Kozyraki R. Cubilin, a high-density lipoprotein receptor. Curr Opin Lipidol. 2000 Apr;11(2):133–40.

40. Röhrl C, Stangl H. HDL endocytosis and resecretion. Biochim Biophys Acta - Mol Cell Biol Lipids. 2013 Nov;1831(11):1626–33.

41. Ji Y, Wang N, Ramakrishnan R, Sehayek E, Huszar D, Breslow JL, et al. Hepatic Scavenger Receptor BI Promotes Rapid Clearance of High Density Lipoprotein Free Cholesterol and Its Transport into Bile. J Biol Chem. 1999 Nov;274(47):33398–402.

42. Calabresi L, Gomaraschi M, Franceschini G. High-Density Lipoprotein Quantity or Quality for Cardiovascular Prevention? Curr Pharm Des. 2010 May;16(13):1494–503.

43. Tall AR, Jiang X, Luo Y, Silver D. 1999 George Lyman Duff Memorial Lecture. Arterioscler Thromb Vasc Biol. 2000 May;20(5):1185–8.

44. Fielding CJ, Shore VG, Fielding PE. A protein cofactor of lecithin:Cholesterol acyltransferase. Biochem Biophys Res Commun [Internet]. 1972 Feb;46(4):1493–8. Available from: https://linkinghub.elsevier.com/retrieve/pii/0006291X72907760

45. Lee J-Y, Parks JS. ATP-binding cassette transporter AI and its role in HDL formation. Curr Opin Lipidol. 2005 Feb;16(1):19–25.

46. Acton S, Rigotti A, Landschulz KT, Xu S, Hobbs HH, Krieger M. Identification of Scavenger Receptor SR-BI as a High Density Lipoprotein Receptor. Science (80-). 1996 Jan;271(5248):518–20.

47. Marcel YL, Kiss RS. Structure-function relationships of apolipoprotein A-I: a flexible protein with dynamic lipid associations. Curr Opin Lipidol. 2003 Apr;14(2):151–7.

48. ANDREWS AL, ATKINSON D, BARRATT MD, FINER EG, HAUSER H, HENRY R, et al. Interaction of Apoprotein from Porcine High-Density Lipoprotein with Dimyristoyl Lecithin. 2. Nature of Lipid-Protein Interaction. Eur J Biochem. 1976 May;64(2):549–63.

49. Segrest JP, Jones MK, De Loof H, Brouillette CG, Venkatachalapathi Y V, Anantharamaiah GM. The amphipathic helix in the exchangeable apolipoproteins: a review of secondary structure and function. J Lipid Res. 1992 Feb;33(2):141–66.

50. Segrest JP, Jackson RL, Morrisett JD, Gotto AM. A molecular theory of lipid-protein interactions in the plasma lipoproteins. FEBS Lett. 1974 Jan;38(3):247–53.

51. Van Lenten BJ, Wagner AC, Navab M, Anantharamaiah GM, Hui EK-W, Nayak DP, et al. D-4F, an Apolipoprotein A-I Mimetic Peptide, Inhibits the Inflammatory Response Induced by Influenza A Infection of Human Type II Pneumocytes. Circulation. 2004 Nov;110(20):3252–8.

52. Nolte RT, Atkinson D. Conformational analysis of apolipoprotein A-I and E-3 based on primary sequence and circular dichroism. Biophys J. 1992 Nov;63(5):1221–39.

53. Borhani DW, Rogers DP, Engler J a, Brouillette CG. Crystal structure of truncated human apolipoprotein A-I suggests a lipid-bound conformation. Proc Natl Acad Sci U S A. 1997;94(23):12291–6.

54. Mei X, Atkinson D. Crystal Structure of C-terminal Truncated Apolipoprotein A-I Reveals the Assembly of High Density Lipoprotein (HDL) by Dimerization*. J Biol Chem [Internet]. 2011 Nov;286(44):38570–82. Available from: https://linkinghub.elsevier.com/retrieve/pii/S002192582050700X

55. Koppaka V, Silvestro L, Engler JA, Brouillette CG, Axelsen PH. The Structure of Human Lipoprotein A-I. J Biol Chem [Internet]. 1999 May 21;274(21):14541–4. Available from: http://www.jbc.org/lookup/doi/10.1074/jbc.274.21.14541

56. Segrest JP, Jones MK, Klon AE, Sheldahl CJ, Hellinger M, De Loof H, et al. A detailed molecular belt model for apolipoprotein A-I in discoidal high density lipoprotein. J Biol Chem. 1999;274(45):31755–8.

57. Silva RAGD, Hilliard GM, Li L, Segrest JP, Davidson WS. A mass spectrometric determination of the conformation of dimeric apolipoprotein A-I in discoidal high density lipoproteins. Biochemistry. 2005;44(24):8600–7.

58. Wu Z, Wagner MA, Zheng L, Parks JS, Shy JM, Smith JD, et al. The refined structure of nascent HDL reveals a key functional domain for particle maturation and dysfunction. Nat Struct Mol Biol. 2007;14(9):861–8.

59. Bhat S, Sorci-thomas MG, Tuladhar R, Samuel MP, Thomas J. NIH Public Access. 2008;46(26):7811–21.

60. Martin DDO, Budamagunta MS, Ryan RO, Voss JC, Oda MN. Apolipoprotein A-I assumes a “looped belt” conformation on reconstituted high density lipoprotein. J Biol Chem. 2006;281(29):20418–26.

61. Wu Z, Gogonea V, Lee X, Wagner MA, Li XM, Huang Y, et al. Double superhelix model of high density lipoprotein. J Biol Chem. 2009;284(52):36605–19.

62. Jones MK, Zhang L, Catte A, Li L, Oda MN, Ren G, et al. Assessment of the validity of the double superhelix model for reconstituted high density lipoproteins: A combined computational-experimental approach. J Biol Chem. 2010;285(52):41161–71.

63. Cooke AL, Morris J, Melchior JT, Street SE, Jerome WG, Huang R, et al. A thumbwheel mechanism for APOA1 activation of LCAT activity in HDL. J Lipid Res [Internet]. 2018;59(7):1244–55. Available from: http://www.jlr.org/lookup/doi/10.1194/jlr.M085332

64. Vickaryous NK, Teh EM, Stewart B, Dolphin PJ, Too CKL, McLeod RS. Deletion of N-terminal amino acids from human lecithin:cholesterol acyltransferase differentially affects enzyme activity toward alpha- and beta-substrate lipoproteins. Biochim Biophys Acta [Internet]. 2003;1646(1–2):164–72. Available from: http://www.ncbi.nlm.nih.gov/pubmed/12637024

65. Lee Y-P, Adimoolam S, Liu M, Subbaiah P V., Glenn K, Jonas A. Analysis of human lecithin–cholesterol acyltransferase activity by carboxyl-terminal truncation. Biochim Biophys Acta - Lipids Lipid Metab [Internet]. 1997 Feb;1344(3):250–61. Available from: https://linkinghub.elsevier.com/retrieve/pii/S000527609600149X

66. Francone OL, Evangelista L, Fielding CJ. Effects of carboxy-terminal truncation on human lecithin:cholesterol acyltransferase activity. J Lipid Res. 1996;

67. Melchior JT, Walker RG, Cooke AL, Morris J, Castleberry M, Thompson TB, et al. A consensus model of human apolipoprotein A-I in its monomeric and lipid-free state. Nat

Struct Mol Biol [Internet]. 2017;(November). Available from: http://www.nature.com/doifinder/10.1038/nsmb.3501

68. Pourmousa M, Song HD, He Y, Heinecke JW, Segrest JP, Pastor RW. Tertiary structure of apolipoprotein A-I in nascent high-density lipoproteins. Proc Natl Acad Sci [Internet]. 2018 May 15;115(20):5163–8. Available from: http://www.pnas.org/lookup/doi/10.1073/pnas.1721181115

69. Huang R, Silva RAGD, Jerome WG, Kontush A, Chapman MJ, Curtiss LK, et al. Apolipoprotein A-I structural organization in high-density lipoproteins isolated from human plasma. Nat Struct Mol Biol [Internet]. 2011;18(4):416–22. Available from: http://www.nature.com/doifinder/10.1038/nsmb.2028

70. Cooke AL, Morris J, Melchior JT, Street SE, Jerome WG, Huang R, et al. A Thumbwheel Mechanism for APOA1 Activation of LCAT Activity in HDL. J Lipid Res [Internet]. 2018 May 17;jlr.M085332. Available from: http://www.jlr.org/content/early/2018/05/17/jlr.M085332.full.pdf

71. Rocco AG, Gianazza E, Calabresi L, Sensi C, Franceschini G, Sirtori CR, et al. Structural features and dynamics properties of human apolipoprotein A-I in a model of synthetic HDL. J Mol Graph Model. 2009;28(4):305–12.

72. Calabresi L, Meng QH, Castro GR, Marcel YL. Apolipoprotein A-I conformation in discoidal particles: Evidence for alternate structures. Biochemistry [Internet]. 1993 Jun 29;32(25):6477–84. Available from: https://pubs.acs.org/doi/abs/10.1021/bi00076a023

73. Jones MK, Gu F, Catte A, Li L, Segrest JP. "Sticky" and "promiscuous", the yin and yang of apolipoprotein A-I termini in discoidal high-density lipoproteins: A combined computational-experimental approach. Biochemistry. 2011;50(12):2249–63.

74. Calabresi L, Tedeschi G, Treu C, Ronchi S, Galbiati D, Airoldi S, et al. Limited proteolysis of a disulfide-linked apoA-I dimer in reconstituted HDL. J Lipid Res [Internet]. 2001 Jun;42(6):935–42. Available from: http://www.ncbi.nlm.nih.gov/pubmed/11369801

75. Sevugan Chetty P, Mayne L, Kan Z-Y, Lund-Katz S, Englander SW, Phillips MC. Apolipoprotein A-I helical structure and stability in discoidal high-density lipoprotein (HDL) particles by hydrogen exchange and mass spectrometry. Proc Natl Acad Sci U S A [Internet]. 2012 Jul 17;109(29):11687–92. Available from: http://www.pnas.org/cgi/doi/10.1073/pnas.1209305109

76. Jones MK, Catte A, Li L, Segrest JP. Dynamics of activation of lecithin:cholesterol acyltransferase by apolipoprotein A-I. Biochemistry. 2009;48(47):11196–210.

77. Rocco AG, Sensi C, Gianazza E, Calabresi L, Franceschini G, Sirtori CR, et al. Structural and dynamic features of apolipoprotein A-I cysteine mutants, Milano and Paris, in synthetic HDL. J Mol Graph Model [Internet]. 2010;29(3):406–14. Available from: http://dx.doi.org/10.1016/j.jmgm.2010.08.002

78. Manthei KA, Yang S, Baljinnyam B, Chang L, Glukhova A, Yuan W, et al. Molecular basis for activation of lecithin:cholesterol acyltransferase by a compound that increases HDL cholesterol. Elife [Internet]. 2018 Nov 27;7:1–61. Available from: https://elifesciences.org/articles/41604

79. Glukhova A, Hinkovska-Galcheva V, Kelly R, Abe A, Shayman JA, Tesmer JJG. Structure

and function of lysosomal phospholipase A2 and lecithin:cholesterol acyltransferase. Nat Commun [Internet]. 2015;6:6250. Available from: http://www.nature.com/doifinder/10.1038/ncomms7250

80. O K, Hill JS, Wang X, McLeod R, Pritchard PH. Lecithin:cholesterol acyltransferase: role of N-linked glycosylation in enzyme function. Biochem J [Internet]. 1993 Sep 15;294(3):879–84. Available from: https://portlandpress.com/biochemj/article/294/3/879/30044/Lecithincholesterol-acyltransferase-role-of

81. Manthei KA, Patra D, Wilson CJ, Fawaz M V., Piersimoni L, Shenkar JC, et al. Structural analysis of lecithin:cholesterol acyltransferase bound to high density lipoprotein particles. Commun Biol [Internet]. 2020;3(1). Available from: http://dx.doi.org/10.1038/s42003-019-0749-z

82. Vickaryous NK, Teh EM, Stewart B, Dolphin PJ, Too CKL, McLeod RS. Deletion of N-terminal amino acids from human lecithin:cholesterol acyltransferase differentially affects enzyme activity toward α- and β-substrate lipoproteins. Biochim Biophys Acta - Proteins Proteomics [Internet]. 2003 Mar;1646(1–2):164–72. Available from: https://linkinghub.elsevier.com/retrieve/pii/S1570963903000050

83. Calabresi L, Pisciotta L, Costantin A, Frigerio I, Eberini I, Alessandrini P, et al. The molecular basis of lecithin: Cholesterol acyltransferase deficiency syndromes: A comprehensive study of molecular and biochemical findings in 13 unrelated Italian families. Arterioscler Thromb Vasc Biol. 2005;25(9):1972–8.

84. Kayser F, Labelle M, Shan B, Zhang J, Zhou M. Methods for treating atherosclerosis. U.S.; US008426358B2, 2013.

85. Freeman LA, Demosky SJ, Konaklieva M, Kuskovsky R, Aponte A, Ossoli AF, et al. Lecithin:Cholesterol Acyltransferase Activation by Sulfhydryl-Reactive Small Molecules: Role of Cysteine-31. J Pharmacol Exp Ther [Internet]. 2017;362(2):306–18. Available from: http://jpet.aspetjournals.org/lookup/doi/10.1124/jpet.117.240457

86. Zuniga FI, Loi D, Ling KHJ, Tang-Liu DD-S. Idiosyncratic reactions and metabolism of sulfur-containing drugs. Expert Opin Drug Metab Toxicol. 2012 Apr;8(4):467–85.

87. Casteleijn MG, Parkkila P, Viitala T, Koivuniemi A. Interaction of lecithin-cholesterol acyltransferase with lipid surfaces and apolipoprotein A-I derived peptides. J Lipid Res. 2018;59.

ACTIVITIES AND PUBLICATIONS

Publications

Guidi, B., M. Planchestainer, M. L. Contente, **T. Laurenzi**, I. Eberini, L. J. Gourlay, D. Romano, F. Paradisi, and F. Molinari. 2018. "Strategic Single Point Mutation Yields a Solvent- and Salt-Stable Transaminase from Virgibacillus Sp. in Soluble Form." *Scientific Reports* 8 (1). doi:10.1038/s41598-018-34434-3. (IF 4.239)

Palazzolo, L., C. Parravicini, **T. Laurenzi**, U. Guerrini, C. Indiveri, E. Gianazza, and I. Eberini. 2018. "In Silico Description of LAT1 Transport Mechanism at an Atomistic Level." *Frontiers in Chemistry* 6 (AUG). doi:10.3389/fchem.2018.00350. (IF 3.656)

Gianazza, E., I. Miller, U. Guerrini, L. Palazzolo, **T. Laurenzi**, C. Parravicini, and I. Eberini. 2019. "What if? Mouse Proteomics After Gene Inactivation." *Journal of Proteomics* 199: 102-122. doi:10.1016/j.jprot.2019.03.008. (IF 3.683)

Palazzolo, L., C. Paravicini, **T. Laurenzi**, S. Adobati, S. Saporiti, U. Guerrini, E. Gianazza, et al. 2019. "SLC6A14, a Pivotal Actor on Cancer Stage: When Function Meets Structure." *SLAS Discovery* 24 (9): 928-938. doi:10.1177/2472555219867317. (IF 2.195)

Pavanello, C., A. Ossoli, M. Turri, A. Strazzella, S. Simonelli, **T. Laurenzi**, K. Kono, et al. 2020. "Activation of Naturally Occurring Lecithin: Cholesterol Acyltransferase Mutants by a Novel Activator Compound." *Journal of Pharmacology and Experimental Therapeutics* 375 (3): 463-468. doi:10.1124/JPET.120.000159. (IF 3.389)

T. Laurenzi, C. Parravicini, L. Palazzolo, U. Guerrini, E. Gianazza, L. Calabresi, I. Eberini. 2020. “rHDL modelling and the anchoring mechanism of LCAT activation.” *Journal of Lipid Research*. 62:100006. doi.org/10.1194/jlr.RA120000843. (IF 4.394)

Rabuffetti, M., P. Cannazza, M. L. Contente, A. Pinto, D. Romano, P. Hoyos, A. R. Alcantara, I. Eberini, **T. Laurenzi**, L. Gourlay, F. Di Pisa, F. Molinari. 2021. "Structural Insights into the Desymmetrization of Bulky 1,2-Dicarbonyls through Enzymatic Monoreduction." *Bioorganic Chemistry* 108. doi:10.1016/j.bioorg.2021.10464. (IF 5.088)

Congress presentations

Supramolecular modelling of an LCAT-rHDL assembly and cholesterol trans-esterification mechanism. **T. Laurenzi**, C. Parravicini, L. Palazzolo, U. Guerrini, L. Calabresi, I. Eberini. New perspectives in pharmacology: from genetics to real life, Val Malenco, 2018.

Deciphering and modelling remyelinating mechanisms induced by clinically-used azole antifungals with exploitable repurposing properties. C. Parravicini, L. Palazzolo, E. Bonfanti, S. Raffaele, **T. Laurenzi**, M. Fumagalli, U. Guerrini, F. Di Renzo, R. Bacchetta, E. Menegola, I. Eberini. Congresso scientifico di AISM e della sua Fondazione, Roma, 2018.

Supramolecular modelling of an LCAT-rHDL assembly and cholesterol trans- esterification mechanism. **T. Laurenzi**, C. Parravicini, L. Palazzolo, U. Guerrini, L. Calabresi, I. Eberini. 9. convegno Next Step, Milano, 2018.

Modellng Molecolare e meccanismo di interazione del complesso LCAT-rHDL. **T. Laurenzi**, C. Parravicini, L. Palazzolo, U. Guerrini, L. Calabresi, I. Eberini. 12. convegno Congresso Nazionale Società Italiana di Terapia Clinica e Sperimentale, Milano, 2018.

Mechanism of LAT1 amino acid antiport: a molecular dynamics simulation of the behaviour of a solute and of an inhibitor. D. Polla, L. Palazzolo, C. Parravicini, **T. Laurenzi**, U. Guerrini, C. Indiveri, E. Gianazza, I. Eberini. Non-Animal Approaches in Science, Ispra, 2019.

Deciphering remyelinating mechanisms induced by clinically-used azole antifungals with exploitable repurposing properties: An in silico approach. U. Guerrini, C. Parravicini, L.

Palazzolo, E. Bonfanti, S. Raffaele, **T. Laurenzi**, M. Fumagalli, F. Di Renzo, R. Bacchetta, E. Menegola, I. Eberini. CCG UGM and Conference, Oxford, 2019.

Mechanism of LAT1 amino acid antiporter: a molecular dynamics simulation of the behaviour of a solute and of an inhibitor. L. Palazzolo, C. Parravicini, **T. Laurenzi**, D. Polla, B. Guastella, U. Guerrini, C. Indiveri, E. Gianazza, I. Eberini. WorkshopBio, Milano, 2019.

Supramolecular modeling of an LCAT-rHDL assembly and cholesterol transesterification mechanism. **T. Laurenzi**, C. Parravicini, L. Palazzolo, U. Guerrini, L. Calabresi, I. Eberini. WorkshopBio, Milano, 2019.

Computational modelling of the LCAT::rHDL molecular recognition mechanism. **T. Laurenzi**, C. Parravicini, L. Palazzolo, U. Guerrini, L. Calabresi, I. Eberini. Spring School III edition, Val Malenco, 2019.

IUBMB Advanced School in *Protein Structure Solution, Prediction and Validation*, Spetzes (Greece), 2019. Member of the organizing committee.

Computational modelling of the LCAT::rHDL complex and bases of LCAT pharmacological activation. **T. Laurenzi**, C. Parravicini, L. Palazzolo, U. Guerrini, L. Calabresi, I. Eberini. New perspectives in pharmacology: from genetics to real life, Spring School IV edition, Val Malenco, 2020.